HHS Public Access

Author manuscript

Nat Neurosci. Author manuscript; available in PMC 2017 February 15.

Published in final edited form as:

Nat Neurosci. 2016 October ; 19(10): 1321–1330. doi:10.1038/nn.4360.

Polycomb repressive complex 2 (PRC2) silences genes responsible for neurodegeneration

Melanie von Schimmelmann[1], **Philip A. Feinberg**[1], **Josefa M. Sullivan**[1], **Stacy M. Ku**[1,2], **Ana Badimon**[1], **Mary Kaye Duff**[1], **Zichen Wang**[2,3], **Alexander Lachmann**[2,3], **Scott Dewell**[4], **Avi Ma'ayan**[2,3], **Ming-Hu Han**[1,2], **Alexander Tarakhovsky**[5], and **Anne Schaefer**[1,*]

[1]Friedman Brain Institute, Department of Neuroscience, Icahn School of Medicine at Mount Sinai, New York, NY 10029

[2]Department of Pharmacological Sciences, Icahn School of Medicine at Mount Sinai, New York, NY 10029

[3]BD2K-LINCS Data Coordination and Integration Center, Icahn School of Medicine at Mount Sinai,, New York, NY 10029

[4]Genomics Resource Center, The Rockefeller University, New York, NY 10065

[5]Laboratory of Immune Cell Epigenetics and Signaling, The Rockefeller University, New York, NY 10065

Abstract

Normal brain function depends on the interaction between highly specialized neurons that operate within anatomically and functionally distinct brain regions. Neuronal specification is driven by transcriptional programs that are established during early neuronal development and remain in place in the adult brain. The fidelity of neuronal specification depends on the robustness of the transcriptional program that supports the neuron type-specific gene expression patterns. Here we show that PRC2, which supports neuron specification during differentiation, contributes to the suppression of a transcriptional program that is detrimental for adult neuron function and survival. We show that PRC2 deficiency in striatal neurons leads to the de-repression of selected, predominantly bivalent PRC2 target genes that are dominated by self-regulating transcription factors normally suppressed in these neurons. The transcriptional changes in PRC2-deficient neurons lead to progressive and fatal neurodegeneration in mice. Our results point to a key role of PRC2 in protecting neurons against degeneration.

*Correspondence and requests for materials should be addressed to A. Schaefer via anne.schaefer@mssm.edu.

Accession codes: Gene Expression Omnibus (GEO) Repository (www.ncbi.nlm.nih.gov/geo) GSE84245

Note: Any Supplementary Information and Source Data files are available in the online version of the paper.

Author contributions: A. Schaefer, A.Tarakhovsky, and M.v.Schimmelmann designed the study. M.v. Schimmelmann, P. Feinberg, J. M. Sullivan, A. Badimon, and M.K. Duff executed the molecular and behavioral experiments, J. M. Sullivan and S.M. Ku performed electrophysiology, M.H. Han designed and performed electrophysiology, S. Dewell performed the Chip seq analysis, Z. Wang, A. Lachmann, and A. Ma'ayan performed the enrichment and network analysis. A. Schaefer, A.Tarakhovsky and M.v. Schimmelmann wrote the manuscript. All authors discussed results and provided input on the manuscript.

Competing Financial Interests Statement: The authors declare no competing financial interests.

Introduction

Neuron-lineage and subtype-specific transcription factors play a critical role in the differentiation and functional specification of neurons during brain development[1,2] and in the adult brain[3]. The transcription factor-driven enforcement of neuronal specification overlaps with the suppression of genes that, in their own right, can drive differentiation of non-neuronal cells or neurons of other types. Much of the negative gene regulation in developing neurons is achieved by the Polycomb repressive complex 2 (PRC2)[4]. The function of the PRC2 is mediated by its enzymatic components, Ezh1 or Ezh2, which catalyze histone H3 lysine 27 di- and tri-methylation (H3K27me2/3)[5,6]. PRC2-mediated H3K27me3 leads to gene silencing[6], which is consistent with the role of the PRC2 in preventing the expression of non-neuronal genes in developing neurons[4].

The presence of the lysine methyltransferases Ezh1 and Ezh2[7] as well as the non-enzymatic PRC2 components Suz12 and Jarid2 in adult neurons (Fig. 1a) suggest that even after the completion of neuronal differentiation, PRC2-mediated gene silencing remains operational in adult neurons. Moreover, the age-dependent increase in the levels of H3K27me3 in adult neurons (Fig.1a) indicates the potential relevance of high levels of H3K27me3 in the maintenance of adult neuronal function. In addition to PRC2, which catalyzes H3K27me3, H3K27me3 levels depend on the H3K27me3 specific demethylases Jmjd3/Kdm6b and Utx/Kdm6a[8], both of which are expressed in adult neurons (Allen Brain Atlas). The levels of neuronal H3K27me3 can be modulated by environmental factors. The activity of the H3K27me3-specific demethylases depends on the intracellular levels of a-ketoglutarate, which can fluctuate significantly in response to neuronal metabolic activity[9]. Additionally, neuronal activation can lead to the phosphorylation of histone H3 at serine 28 (H3S28) followed by the dissociation of the PRC2 from chromatin and an ensuing loss of H3K27me3[10]. Changes in PRC2 activity and alterations in H3K27me3 levels and distribution have recently been implicated in several human neurodegenerative diseases[11,12], including Huntington disease (HD)[13,14]. Recent studies identified the PRC2 as a direct target for the huntingtin protein[13]. Moreover, the expression of mutant huntingtin in mouse ES cells or neuronal progenitor cells (NPCs) alters the pattern of genome-wide H3K27me3 distribution in both cell types[15]. The possible link between PRC2 and HD is further supported by the loss of neuronal PRC2/H3K27me3 sites[14] and the up-regulation of some of the PRC2 target genes in the HD affected human brain[14,16,17]. While these studies suggest that the PRC2 might represent a common target of different pathological processes that drive neurodegenerative diseases, the role of the PRC2 in the regulation of neuronal specification, function and survival in the adult brain is not known.

To address the significance of the PRC2 in adult neurons *in vivo*, we have generated mice with a PRC2 deficiency in highly specialized medium spiny neurons (MSNs) in the striatum. We found that the PRC2 is essential for the MSN-specific gene expression and function. The deficiency in PRC2 directly impacts a selected group of PRC2 target genes that encode transcription factors normally suppressed in MSNs as well as death promoting proteins. The ectopic expression of non-MSN and non-neuronal lineage specific transcription factors in PRC2-deficient MSNs is associated with a down-regulation of genes that are required for

MSN-specific functions. These collective changes in gene expression are accompanied by altered neuronal physiology and the development of progressive and fatal neurodegeneration.

Results

Conditional inactivation of the PRC2 in adult neurons

PRC2 deficiency in MSNs has been accomplished by combining a null-mutation in the *Ezh1* gene (*Ezh1*$^{-/-}$) with the conditional ablation of the *Ezh2* gene in different types of neurons (Supplementary Fig. 1a). To achieve the forebrain neuron-specific *Ezh2* gene inactivation, we combined *Ezh2*$^{fl/fl}$ [18] and *Camk2a-Cre* alleles in *Ezh2*$^{fl/fl}$*; Camk2a-Cre* mice, which allow Cre-mediated recombination of *loxP*-modified genes in projection neurons in the striatum, cortex, and hippocampus at 2 weeks of age. Neuronal development and maturation are associated with a switch from a predominantly Ezh2 to a mostly Ezh1 containing PRC2 (Fig. 1a). However, neither Ezh1 nor Ezh2 deficiency (Supplementary Fig. 1b) alone has an impact on the overall levels or the genome-wide distribution of H3K27me3 (Fig. 1b, c), and only the combined Ezh1 and Ezh2 deficiencies lead to a loss of H3K27me3 in MSNs in the striatum (Fig. 1b-d). The global loss of H3K27me3 in the MSNs becomes evident around 6 weeks of age and approximately 3-4 weeks after PRC2 inactivation (Fig. 1d). As expected, the H3K27me3 deficiency in *Ezh1*$^{-/-}$*; Ezh2*$^{fl/fl}$*; Camk2a-cre* mice is strictly neuron specific. The glia cells from these mice express wild type levels of H3K27me3 (Fig. 1d).

The delayed, with respect to the timing of PRC2 inactivation, ablation of H3K27me3 in MSNs suggests that most of the postnatal MSN development in *Ezh1*$^{-/-}$*; Ezh2*$^{fl/fl}$*; Camk2a-cre* mice occurs in the presence of wild type-like H3K27me3 levels. This finding argues against a possible developmental impact of the PRC2 deficiency on adult MSN gene expression in *Ezh1*$^{-/-}$*; Ezh2*$^{fl/fl}$*; Camk2a-cre* mice.

To inactivate PRC2 specifically in specialized adult neurons, we have limited the inactivation of the PRC2 to specific neuron types. In particular, we have generated mice with PRC2 inactivation specifically in dopamine D1 or D2 receptor expressing neurons. This has been achieved by breeding *Drd1a-Cre* or *Drd2-Cre* mice to the *Ezh1*$^{-/-}$*; Ezh2*$^{fl/fl}$ mice (Supplementary Fig. 1a.). To exclude any potential developmental impacts of the PRC2 ablation, we use an AAV-based approach to inactivate the PRC2 in the striatum of 10-week old *Ezh1*$^{-/-}$*; Ezh2*$^{fl/fl}$ mice (Supplementary Fig. 1a). Finally, we employ the Purkinje cell specific Cre-expressing mouse strain *Pcp2-cre* to inactivate the PRC2 in postnatal cerebellar Purkinje cells (Supplementary Fig. 1a). The details of the neuron type-specific inactivation of the PRC2 will be discussed below in the context of the cell-type specific impact of PRC2 deficiency on gene expression and cell function.

PRC2 targets non-neuronal, non-MSN and death-promoting genes in adult MSNs

To elucidate the role of the PRC2 in the regulation of neuronal cell type-specific gene expression, we first have identified the PRC2 target genes in MSNs of adult mice. To address the chromatin state of genes in MSNs, we have conducted our studies on highly purified *ex vivo* isolated MSN nuclei (Supplementary Fig. 2a) We found that genes

associated with H3K27me3 in adult MSNs are transcriptionally silent and lack Pol II or the activation associated H3K27acetyl at the transcriptional start sites (TSS) (Fig. 2a, b). The majority of the H3K27me3 enriched genes include genes that are normally expressed either in cells of non-neuronal lineages or in non-MSN neurons (Fig. 2c).

A large fraction of H3K27me3-enriched (FPKM > 1.2, Supplementary Table 1) and transcriptionally silent genes in MSNs possess H3K4me3 at their TSS, which is commonly associated with transcriptional activity[19] (Fig. 2b, d, e, Supplementary Table 2). The simultaneous presence of H3K27me3 and H3K4me3, which is defined as chromatin bivalency[20,21], has been validated by the sequential immunoprecipitation of H3K27me3 associated chromatin from *ex vivo* isolated adult MSNs followed by H3K4me3 immunoprecipitation (Fig. 2f). Approximately 65% (544/835, $P < 0.0001$) of the bivalent genes in MSNs overlap with genes that have been previously identified as bivalent in ES cells[21,22], while the rest of the bivalent genes are MSN specific (Supplementary Fig. 2b).

The most abundant class of bivalent loci in MSNs is represented by genes that encode transcriptional regulators associated with non-MSNs as well as with non-neuronal cells (Fig. 2 g). Notably, the MSN bivalent genes include genes that encode important regulators of cell death (Fig. 2g), such as *Pmaip1/Noxa, Bik, Cdkn2a/b, Trp73, Gas1, Wt1* and *Ccnd1* (Supplementary Table 2).

Selective PRC2 target gene up-regulation in the absence of the PRC2

The PRC2 targets thousands of genes in adult MSNs (Fig. 2a). However, the deficiency in PRC2 leads to highly selective changes in MSN gene expression that occur with a significant delay after the onset of H3K27me3 deficiency. While MSNs in the striatum of six week-old *Ezh1*$^{-/-}$*; Ezh2*$^{fl/fl}$*; Camk2a–cre* mice display no changes in gene expression (Fig. 3a), we observe upregulation of PRC2 target genes at three months of age (Fig. 3a). By six months of age, we observe an increase in both the number (Fig. 3a) and expression levels (Fig. 3b, left panel) of up-regulated genes in MSNs. The majority of up-regulated genes are direct targets of H3K27me3 (Fig. 3b right panel, Supplementary Fig. 3a), and more than 50% display a bivalent chromatin state in wild type MSNs (Fig. 3b, right panel, Supplementary Table 3). These data suggest that PRC2 plays a specific role in the suppression of bivalent genes in MSNs but does not explain the selectivity and time–dependent up-regulation of PRC2 target genes.

The up-regulated genes are greatly enriched for genes encoding non-MSN-expressed transcriptional regulators (Fig. 3c, Supplementary Fig. 3a, Supplementary Table 4), which are expressed at levels sufficient for *in situ* detection in the mutant neurons (Fig. 3d). The majority of the induced transcriptional regulators encode homeobox genes including numerous Hox genes (Fig. 3e) that are normally silenced in MSNs during early developmental stages.

The transcriptional control of more than 25% of the transcriptional regulators that become up-regulated in the absence of the PRC2 entails the formation of positive auto-regulatory feedback loops as described in the earlier studies or as identified by the analysis of cis-regulatory elements (oPPOSUM and GENOMATIX analysis) (Fig. 3e, Supplementary Table

5). A large fraction of the transcriptional regulators that become up-regulated in PRC2-deficient MSNs have experimentally proven (Fig. 3e, right panel, Supplementary Fig. 3b) or sequence-predicted (Supplementary Table 5) co-regulatory functions that may allow the formation of transcriptional networks reinforcing the expression of these genes. Our data suggest that while the majority of H3K27me3 target genes in MSNs are surprisingly insensitive to PRC2 deficiency, a selective group of predominantly bivalent PRC2 targets become expressed at relatively high levels due to the ability to form mutually reinforcing transcriptional network(s). The formation of self-controlled mutually reinforced transcription loops among PRC2 target genes represents a possible mechanism for the selective and progressive up-regulation of PRC2 target genes.

PRC2 deficiency is associated with a down-regulation of MSN–specific genes

The ectopic expression of the PRC2 target genes in MSNs is associated with a concurrent down-regulation of 119 MSN-expressed genes in *Ezh1*$^{-/-}$*; Ezh2*$^{fl/fl}$*; Camk2a–cre* mice (Fig. 3a, Supplementary Fig. 4a). The down-regulated genes are not associated with H3K27me3 in wild-type MSNs and hence cannot be directly regulated by the PRC2 (Supplementary Fig. 4b). The down-regulated genes are significantly enriched (38/119, $P < 0.0001$, Odds Ratio: 25.16) for key regulators of MSN identity and specialized functions[23,24] (Fig. 4a-c; Supplementary Table 6). PRC2-deficient MSNs display reduced expression levels of genes that encode important regulators of MSN-specific functions (Fig. 4a), including neurotransmitter receptors (*Drd2*, *Drd1a*, *Adora2a*,), signaling proteins (*Arpp21*, *Rgs9*, *Pde10a*), and MSN-specific transcription factors (*Rxrg*, *Foxp1*) (Fig. 4b). Many of the down-regulated genes have been linked to neurological disease processes in humans (Supplementary Fig. 4 c). The reduced expression of selected MSN genes is highly specific and is in contrast to the wild type-like expression levels of the majority of MSN-expressed genes (Fig. 4c). The PRC2-deficient D2 MSNs, while present at wild type numbers in the striatum of 5 month-old mutant mice, express significantly lower levels of the D2 MSN-specific gene *Drd2* as compared to control D2 MSNs (Fig. 4d).

Based on the known pattern of *Camk2a* expression in neurons, the conditional PRC2 deficiency may affect not only MSNs but also other forebrain projection neurons, including layer 5/6 cortical neurons, which directly innervate MSNs[25]. It is therefore conceivable that the down-regulation of MSN-specific genes could reflect changes in their cortical innervation. To address this possibility, we have employed mice with D1 or D2 neuron-specific PRC2 inactivation. The *Ezh1*$^{-/-}$*; Ezh2*$^{fl/fl}$*; Drd1-Cre* or *Ezh1*$^{-/-}$*; Ezh2*$^{fl/fl}$*; Drd2-Cre* mice were bred to *Drd1-TRAP* or *Drd2-TRAP* mice (Supplementary Fig. 5a) for D1- or D2-neuron specific ribosome-associated mRNA analysis[23]. The D1 or D2 MSN-specific PRC2 deficiency leads to the up-regulation of the same PRC2 target genes as well as a down-regulation of MSN specific genes that are observed in the MSNs of *Ezh1*$^{-/-}$*; Ezh2*$^{fl/fl}$*; Camk2a–cre* mice (Supplementary Fig. 5a). These findings support the MSN cell-intrinsic nature of transcriptional changes that follow PRC2 deficiency in MSNs. An additional proof for the role of PRC2 in the maintenance of adult MSN gene expression has been obtained by using *AAV-Cre* mediated inactivation of the PRC2 in adult neurons. The dorsal striatum specific injection of *AAV-Cre-eGFP* leads to a loss of H3K27me3 in the virus-infected MSNs of the *Ezh1*$^{-/-}$*; Ezh2*$^{fl/fl}$ mice but not control mice (Supplementary Fig. 5b). The

PRC2 deficiency induced in adult MSNs is associated with changes in MSN gene expression similar to the changes observed in the *Ezh1*$^{-/-}$*; Ezh2*$^{fl/fl}$*; Camk2a–cre* mice or in PRC2 deficient D1 or D2 neurons (Supplementary Fig. 5a, c).

PRC2-silences death-promoting genes

One of the distinct classes of PRC2 target genes in the MSNs of wild type mice is represented by death-promoting genes (Fig. 2g, indicated by a star). We found that PRC2 deficiency in MSNs leads to an up-regulation of PRC2 target genes, such as *Pmaip1/Noxa, Bid, Cdkn2a/b,* and *Igfbp3* (Fig. 5a), which have a well-known role in the control of cell survival by promoting cell death[26]. Moreover, we observe an increased expression of the direct PRC2 target genes *Ccnd1,* which can trigger neuronal death *in vitro*[27] and has been implicated in several neurodegenerative processes[28], and *Wt1*, a mediator of neuronal degeneration associated with Alzheimer's disease[29] (Fig. 5a). The PRC2-dependent death-promoting genes also become up-regulated in PRC2 deficient D1 or D2 neurons (Supplementary Fig. 6, left), and in adult striatal neurons following *AAV-Cre* mediated PRC2 inactivation (Supplementary Fig. 6, right).

PRC2 deficiency in MSN causes a progressive and fatal neurodegenerative phenotype

Concomitantly with the increased expression of death–promoting genes, the PRC2 deficient MSNs in six month-old *Ezh1*$^{-/-}$*; Ezh2*$^{fl/fl}$*; Camk2a–cre* mice display a significant increase in γH2ax (Fig. 5b-c). γH2ax is a marker of DNA double strand breaks and DNA damage that have been linked to neurodegeneration in mice and in humans[30-32]. Moreover, electron microscopy analysis revealed multiple abnormal MSNs that display nuclear and cytoplasmic condensation in the presence of intact subcellular organelles (Fig. 5d). This phenotype, which is known as dark cell degeneration, is a hallmark of neurodegeneration[33]. The cellular alterations of PRC2 deficient MSNs are accompanied by a significant reduction in both the total brain mass (Fig. 5e, left) and the number of MSNs (Fig. 5e, right) in the striatum of the mutant mice.

The down-regulation of MSN-specific genes, the up-regulation of the death-promoting PRC2 target genes, and the morphological signs of neurodegeneration are intertwined with alterations in MSN physiology (Fig. 6). The PRC2-deficient MSNs display enhanced intrinsic excitability with a significant increase in evoked action potential firing (Fig. 6a), reduced firing threshold (reduced rheobase) (Fig. 6b), and an increased input resistance (Fig. 6c).

The described changes in PRC2 deficient MSNs are associated with altered behavior. The *Ezh1*$^{-/-}$*; Ezh2*$^{fl/fl}$*; Camk2a–cre* mice develop a fatal neurodegenerative condition characterized by progressively attenuated motor activity and balance. The altered motor functions are associated with impaired rotarod performance (Fig. 6d), impaired ability to hang on a wire top (Supplementary Fig. 7a), and hind limb clasping behavior (Fig. 6e) followed by a complete cessation of voluntary motor activity including feeding or drinking behavior in the home cage (Supplementary Fig. 7b). These changes result in the premature death of mice around 6.5-7 month of age (Fig. 6f).

It is possible that some aspects of the observed behavioral changes in *Ezh1*$^{-/-}$*; Ezh2*$^{fl/fl}$*; Camk2a–cre* mice reflect alterations in cortical neurons rather than MSN-autonomous changes. In support of the cell-autonomous role of the PRC2 in the regulation of MSN function, we found that the virus-mediated loss of the PRC2 specifically in adult striatal neurons leads to a progressive impairment in motor behavior (Fig. 6g- h). Moreover, the loss of PRC2 in both D1 and D2 neurons is associated with the premature death of the mutant mice (Fig. 6i). These data support a MSN-autonomous role of the PRC2 in the regulation of MSN function.

PRC2 controls Purkinje cell (PC) specific gene expression and survival

The neurodegeneration caused by PRC2 deficiency is not uniquely restricted to neurons in the forebrain. The loss of the PRC2 in postnatal cerebellar PC impairs the PC phenotype (Fig. 7). The alterations in gene expression in PRC2-deficient PCs follow a similar pattern of gene expression changes observed in the PRC2-deficient MSNs (Fig. 7b). The PC-specific TRAP analysis of *Ezh1*$^{-/-}$*; Ezh2*$^{fl/fl}$*; Pcp2-cre*; *Pcp2-TRAP* mice reveals that PRC2-deficient PCs up-regulate PRC2 target genes. Many of these genes include the same transcriptional regulators that are up-regulated in PRC2-deficient MSNs (Fig. 7b). As in PRC2-deficient MSNs, the de-repression of the PRC2 target genes is associated with the down-regulation of genes that are critical for PC function and survival (Fig. 7b, right panel). The reduced expression of genes controlling PC function and survival may augment the effect of potential death-promoting PRC2 target genes that are up-regulated in PRC2-deficient PCs (Fig. 7b). Similar to PRC2 deficient MSNs, the changes in PC specific gene expression are associated with a progressive loss of PCs and an accompanying impairment in motor behaviors (Fig. 7a, c, d). We observe a significant, age-dependent decrease in the size of the molecular layer (Fig. 7d, left), followed by a significant reduction in the number of PC bodies at nine month of age (Fig. 7d, right). These data support the general relevance of the PRC2 in the maintenance of adult neuron function and survival.

Discussion

PRC2-mediated H3K27me3 is one of the hallmarks of developmentally determined gene silencing that critically contributes to the differentiation of cells of various types [6,34]. Our studies address the role of the PRC2 in adult neurons where neuronal lineage specification is associated with highly specialized neuron type-specific gene expression programs[23,35]. We show that the maintenance of H3K27me3 in adult neurons requires the presence of either Ezh1 or Ezh2, which represent homologous but structurally distinct enzymatic components of the PRC2[5]. Although Ezh2 expression levels decline sharply during early postnatal brain development[7], this enzyme is able to compensate for a deficiency in Ezh1, which dominates the PRC2 in adult neurons (Fig. 1a). The redundancy between Ezh1 and Ezh2 may reflect specific features of post-mitotic neurons since Ezh1 cannot substitute Ezh2 in dividing cells during brain development[6].

In MSNs, H3K27me3 remains at wild type levels for at least 2 weeks after ablation of the PRC2. The stability of H3K27me3 in neurons does not reflect the existence of another, not yet identified H3K27me3 specific histone methyltransferase, as deficiency in Ezh1/2

ultimately leads to H3K27me3 loss. The durability of H3K27me3 in the absence of the PRC2 cannot be attributed to the lack of expression of the H3K27me3 specific demethylases Jmjd3 and Utx. Both enzymes are expressed at wild type levels in PRC2-deficient MSNs (data not shown). In the most likely scenario, the stability of H3K27me3 reflects the low rate of histone H3 turnover in non-dividing cells including neurons[36,37] in combination with the slow kinetics of lysine demethylation by Jmjd3 and Utx[38].

We identified 2057 PRC2 target genes in MSNs, which are associated with high levels of H3K27me3 at their TSS. Many of these PRC2 targeted gene are associated with H3K27me3/HK4me3 bivalent chromatin (835/2057). In ES cells as well as in cells of other types, the chromatin bivalency supports the plasticity of cell differentiation[39-41]. However, it is unlikely that fully differentiated MSNs could benefit from the expression of genes that can potentially alter MSN differentiation and function. It is possible that the bivalent state of these transcriptional regulators is a reflection of their specific DNA sequence. A majority of bivalent promoters contain CpG islands[40], and the PRC2 is commonly recruited to GC-rich sequence elements[42,43].

The TSS-associated H3K4me3 is not only an indicator of a gene's transcriptional potential but can also be a marker of promoter-associated transcription. In turn, it has been shown that transcription can promote the recruitment of the PRC2 [44]. Therefore, it is possible that the presence of H3K4me3 is required for the recruitment of the PRC2 and subsequent gene silencing. One can envision a scenario in which the presence of H3K4me3 on bivalent genes may support low levels of transcriptional activity, i.e. promoter-associated transcription, which may not yield the full-length RNA but is necessary and sufficient for the recruitment and/or maintenance of the PRC2 required for gene silencing.

Our data suggest that the function of PRC2 in adult neurons lies in the suppression of bivalent genes, while the majority of H3K27me-associated gene suppression does not depend on PRC2 activity. The necessity of PRC2 for bivalent gene silencing in adult neurons is consistent with a similar role of PRC2 in bivalent gene suppression-mediated patterning of the tissue-specific gene expression patterns in the adult mouse intestine, blood, and skin cells[45].

The PRC2 deficiency in MSNs leads to a surprisingly delayed -with respect to the timing of the onset of the H3K27me3 deficiency- up-regulation of a limited group of bivalent PRC2 targets that are enriched for genes encoding other cell/neuron type-specific transcriptional regulators. These selective changes in gene expression may reflect the ability of many of the up-regulated transcription factors to form auto- or co-regulatory transcriptional networks. It is possible that loss of H3K27me3 and the ensuing acquisition of H3K27Ac may lead to a transcriptionally promiscuous state of a large number of PRC2 targets. However, only those that can form auto-/co-regulatory networks will reach detectable RNA expression levels over time. The selective up-regulation of genes in PRC2 deficient cells may therefore reflect not only the role of H3K27me3 in transcriptional silencing but also the specific transcriptional features of the de-repressed PRC2 gene targets. Our data suggest that the H3K27me3 target genes may not be particularly sensitive to PRC2 deficiency but may become expressed at

relatively high levels due to the ability to form mutually reinforcing transcriptional network(s).

The slow, age-dependent up-regulation of non-MSN specific transcriptional regulators does not lead to an induction of other cell/neuron type-specific gene programs but is associated with the subsequent down-regulation of MSN-specific genes. The PRC2-dependent changes in MSN gene expression, physiology, and survival, while having distinct mechanistic foundations, are likely to reinforce each other causing progressive and fatal neurodegeneration. For example, the ectopic expression of *Ccnd1*, which is associated with excitotoxic neuronal death, and *Wt1,* which is implicated in mediating neuronal degeneration in AD, can trigger cell death in neurons *in vitro*[27-29]. At the same time, attenuated expression of MSN-specific neurotransmitter receptors and ion channels, such as *Kcnd2,* in PRC2 deficient MSNs can lead to pathological neuronal excitability, which may initiate secondary PRC2-independent events that promote cell death in a cell-intrinsic or -extrinsic fashion. The neurodegenerative process, while initially triggered by PRC2-deficiency, may progress with the help of PRC2 independent mechanism. This scenario could preclude the identification of a single factor downstream of PRC2 that is responsible for the progression of neurodegeneration.

The progressive neurodegeneration in mice lacking the PRC2 in MSNs or PCs reinforces the notion of the involvement of PRC2 in neurodegenerative diseases in humans. We found that the loss of the PRC2 in adult forebrain neurons leads to HD-like changes in gene expression (Supplementary Fig. 3a, Supplementary Fig. 8). 20-30% of the PRC2-target genes that become up-regulated in PRC2-deficient MSNs, including *Pou4f1/2, Hand2, Nkx2-5*, *Twist1*, *Tal1, Wt1*, and numerous *Hox* genes, significantly overlap with genes that are up-regulated in the postmortem human brains of HD patients[14,16,17] or HD mouse models[46,47] (Supplementary Fig. 8, Supplementary Table 7).

Similarly to the up-regulated genes, ~50% of the genes that become down-regulated in PRC2 deficient MSNs (54/119, $P < 0.001$, Supplementary Table 7) significantly overlap with genes that are down-regulated in the brain of HD patients or mouse models of the disease[46,47] (Supplementary Fig. 4c).

In addition to the overlap in gene expression, PRC2 deficient MSNs display alterations in MSN physiology in a fashion that resembles mouse MSNs affected by HD[48]. Similar to HD-affected neurons[48], PRC2-deficient MSNs display enhanced intrinsic excitability in combination with increased input resistance. Moreover, cellular alterations, including the presence of γH2ax loci and the dark cell degeneration phenotype, are reminiscent of neurodegeneration in HD in mice and in humans[30,31,33]. Concurrent with the alterations in MSN-specific gene expression and function, mice with a forebrain neuron specific PRC2 deficiency develop progressive and fatal neurodegeneration that is similar to HD in mice and in humans[49]. Despite obvious phenotypic similarities between molecular, cellular and behavioral defects caused by neuronal PRC2 deficiency and neurons affected by HD, it would be naïve to equate these two conditions. HD is a complex disorder in which the mutant huntingtin protein can affect various cytoplasmic as well as nuclear processes that collectively contribute to MSN degeneration. However, our data give more credence to the

contribution of epigenetic mechanisms, particularly to PRC2-mediated gene expression regulation, in HD pathology and possibly in other neurodegenerative processes.

The general relevance of the PRC2 in neurodegenerative processes is further supported by studies that show changes in PRC2 activity and a genome-wide redistribution of H2K27me3 during ATM deficiency[11] and a de-repression of PRC2 target genes in a mouse model of Parkinson's disease[12].

In summary, our data reveal the important role of the PRC2 in the maintenance of adult neuron specification, function and survival. Exposure to cell extrinsic or intrinsic stressors that can alter neuronal activity and/or metabolism may destabilize the neuronal subtype-specific gene expression patterns by affecting the bivalent state of non-neuronal genes or genes of other neuronal types. As discussed, changes in PRC2 function could be triggered either transiently, by non-persisting events such as seizures [50], or permanently, by the expression of pathogenic proteins such as mutant huntingtin protein, which can directly interfere with PRC2 recruitment and function[13,14]. In view of our findings, the presence of the large number of self-regulatory transcription factors among PRC2 targets suggest that changes in proteins that control H3K27me3 levels or chromatin distribution globally or locally can trigger self-propagating transcriptional processes that set neurons on a path of neurodegeneration. Altered neuron specification may interfere with coordinated function of neuronal networks and may be harmful for overall brain function. It is plausible that neurons possess an intrinsic mechanism that triggers the elimination of neurons with defective specification during development. It is tempting to speculate that the activation of the PRC2-controlled death-promoting genes may represent this check-point mechanism that enables the elimination of neurons with impaired PRC2 function. While short-term activation of such a mechanism could be beneficial for ensuring brain integrity, persistent changes in the activity or recruitment of PRC2, as well as other H3K27me3 controlling enzymes, may lead to systemic neurodegeneration.

Methods

Animals

Mice were housed at two to five animals per cage with a 12-hour light/dark cycle (lights on from 0700 to 1900 hours) at constant temperature (23 °C) with *ad libitum* access to food and water. All animal protocols were approved by the Institutional Animal Care and Use Committee (IACUC) at the Icahn School of Medicine at Mount Sinai.

Generation of neuron-specific Ezh2 and Ezh1/Ezh2 conditional knock-out and control mice

Ezh2$^{fl/fl}$ mice were bred to *Camk2a-cre* (kindly provided by G. Schütz[51], German Cancer Research Center, Heidelberg) or *Pcp2-cre* mice[52,53]. *Ezh1*$^{-/-}$ mice (kindly provided by T. Jenuwein[54], Max Planck Institute, Freiburg) were crossed with *Ezh2*$^{fl/fl}$*; Camk2a-Cre* or *Ezh2*$^{fl/fl}$*; Pcp2-Cre* mice to generate combined *Ezh1*$^{-/-}$*; Ezh2*$^{fl/fl}$*; Camk2a-Cre* or *Ezh1*$^{-/-}$*; Ezh2*$^{fl/fl}$*; Pcp2-Cre* mice, respectively.

If not otherwise specified, *Ezh1*$^{-/-}$, *Ezh2*$^{fl/fl}$, and *Ezh1*$^{-/-}$*; Ezh2*$^{fl/fl}$ mice were used as controls for *Ezh1*$^{-/-}$, *Ezh2*$^{fl/fl}$*; Camk2a-Cre,* and *Ezh1*$^{-/-}$*; Ezh2*$^{fl/fl}$*; Camk2a-Cre*, respectively after

excluding any changes in gene expression or motor behavior in *Ezh1*$^{-/-}$, *Ezh2*$^{fl/fl}$, *Ezh1*$^{-/-}$; *Ezh2*$^{fl/fl}$; *Camk2a-Cre* or *Pcp2-Cre* transgenic mice as compared to wild type littermate controls.

Ezh1$^{-/-}$; *Ezh2*$^{fl/fl}$ were bred to *Drd1-Cre* or *Drd2-Cre* mice[23,55] to generate *Ezh1*$^{-/-}$; *Ezh2*$^{fl/fl}$; *Drd1a-cre* and *Drd2-cre; Ezh1*$^{-/-}$; *Ezh2*$^{fl/fl}$; *Drd2-Cre* mice, respectively. Additionally, *Ezh1*$^{-/-}$; *Ezh2*$^{fl/fl}$ were bred to *Drd1-Cre; Drd1-TRAP* or *Drd2-Cre; Drd2-TRAP* mice[23,55] to generate *Ezh1*$^{-/-}$; *Ezh2*$^{fl/fl}$; *Drd1a-cre; Drd1-TRAP* and *Drd2-cre; Ezh1*$^{-/-}$; *Ezh2*$^{fl/fl}$; *Drd2-Cre; Drd2-TRAP*, and control *Ezh1*$^{+/-}$; *Ezh2*$^{fl/fl}$; *Drd1-TRAP* and *Ezh1*$^{+/-}$; *Ezh2*$^{fl/fl}$; *Drd2-TRAP* mice, respectively.

Ezh1$^{-/-}$; *Ezh2*$^{fl/fl}$; *Pcp2-Cre* mice were crossed to *Pcp2-TRAP* mice (kindly provided by N.Heintz[35], The Rockefeller University, New York) to generate *Ezh1*$^{-/-}$; *Ezh2*$^{fl/fl}$; *Pcp2-Cre; Pcp2-TRAP* and control *Ezh1*$^{+/-}$; *Ezh2*$^{fl/fl}$; *Pcp2-TRAP* mice. All mice used for experiments were backcrossed to the C57Bl/6 background for ≥ 5 generations.

Surgery/AAV injection

To induce deletion of Ezh2 in adult MSNs, neurotrophic Adeno-associated virus (1μl of 10^{12} AAV serotype 5) expressing eGFP-Cre under the control of a *CMV* promoter (*AAV5-cre; eGFP*; Vector Biolabs) was stereotaxically injected into the dorsal striatum of *Ezh1*$^{-/-}$; *Ezh2*$^{fl/fl}$ and control mice at 10 weeks of age. The stereotactic surgery was performed as previously described[56]. The efficiency of Cre-mediated recombination was verified by immnohistochemical analysis of H3K27me3.

Purification of *ex vivo* cell-type specific nuclei from mouse brain

Purification of nuclei from mouse striatum was achieved as previously described[57,58] with minor modifications. Briefly, striata of 8 week old C57Bl/6 mice were quickly dissected and homogenized with a glass dounce homogenizer (Kimble Chase; 1984-10002). After fixation of the cell homogenate with a final concentration of 1% formaldehyde for eight minutes at room temperature and quenching of the reaction with 0.125 M Glycine for five minutes at room temperature, the fixed homogenate was spun through a 29% iodixanol cushion. The resulting nuclei pellet was resuspended in resuspension buffer (0.25 M sucrose, 25 mM KCl, 5 mM MgCl2, 20 mM Tricine pH 7.8, 0.15 mM spermine, 0.5 mM spermidine, EDTA-free protease inhibitor cocktail (Roche, 11836170001)) supplemented with 10 μM DyeCycle Ruby (Invitrogen, V10304), 10% Donkey Serum (JacksonImmuno Research, 017-000-121) and 1:10,000 NeuN antibody conjugated to Alexa488 (Millipore, MAB377X). After incubation in resuspension buffer for one hour on ice, nuclei were subject to *Fluorescence-activated cell sorting* (FACS). Two-dimensional gating criteria were used as previously described[57]. Since NeuN is a neuronal marker[59], nuclei fractions with an Alexa488 signal above the background were considered neuronal nuclei fractions, while those with an Alexa488 signal below the background were considered glial nuclei fractions (Supplementary Fig. 2a). After sorting, nuclei were pelleted at 2,000 g for 15 minutes and stored at -80 °C until further analysis.

Chromatin immunoprecipitation (ChIP)

Antibodies against H3K27me3 (Millipore, 07-449), H3K27ac (Abcam, ab4729), RNA polymerase II (Abcam, ab5408), and H3K4me3 (Abcam, ab8580) were bound to Protein G magnetic beads (Diagenode, kch-818-220) for two hours at 4 °C (50 μl Protein-G magnetic beads were incubated with 15 μg of antibody). DNA from sorted nuclei fractions (1×10^6 nuclei (equivalent to 10 mice each) for each ChIP) was sonicated for 12 cycles of 30 s On/30 s Off at 4 °C on high power to fragments of a size range of 200 to 500 bp with a Bioruptor (Diagenode). After removal of an input sample equivalent to 1% of each ChIP reaction, sheared chromatin was immunoprecipitated with 50 μl Protein G-bound antibodies (15 μg) using the LowCell ChIP kit (Diagenode, kch-maglow-G48) in the presence of protease inhibitors and the HDAC inhibitor sodium butyrate (Diagenode, kch-817-001) for 24 hours at 4 °C. After incubation, chromatin pulled down by the Protein G-bound antibodies was washed and immediately cleaned up with the IPure kit (Diagenode, AL-100-0100). The unbound fraction of the immunoprecipitation reaction was used to validate the fragmentation on a 1% agarose gel. Purification with the IPure kit was carried out according to the manufacturer's instructions with the addition of Proteinase K treatment (Roche, 03115828001) for one hour at 55 °C after the de-crosslinking step. Immune-enriched chromatin was further purified with phenol/chloroform/isoamylalcohol (25:24:1) and concentrated by ethanol precipitation. ChIP-sequencing libraries were prepared using the ChIP-Seq DNA sample preparation kit (Illumina, IP-102-1001) using an adapter oligo dilution of 1:25 for all samples. Prepared samples were amplified onto flowcells using the Illumina Cluster Station or cBot per manufacturer protocol and sequenced on either the Illumina GAIIx for 36 cycles or the HiSeq 2000 platform for 50 cycles. Raw sequencing data was processed using the onboard SCS/RTA software yielding 36 bp reads for GAIIx data. Datasets from the HiSeq 2000 platform were trimmed back to 36 bp to compare with the GAIIx data.

ChIP-Sequencing analysis

Sequences were aligned using bowtie v0.12.7, allowing for ≤ 2 mismatches to the reference in 36bp. We generated sets of high quality and uniquely (< 60%) aligned reads for H3K27me3, H3K4me3, PolII, and H3K27acetyl from wild-type C57Bl/6 neuronal and glia nuclei. For the Ezh1 and Ezh2 and Ezh1/2 mutant MSN nuclei, ChIP sequencing experiments yielded high quality and uniquely aligned reads (< 60%) for H3K27me3. Uniquely mapped reads were used for subsequent analysis. Browser files were made with IGV Tools using the count option, extending the reads 100 bp to account for the anticipated size of the immunoprecipitated fragments. Peak calling was performed using MACS v1.4, and CCAT v3.0. ChIP-Seq profiles were created by counting the number of reads in 50 bp bins upstream and downstream of the indicated genomic feature for the length indicated on the x-axis. TSS coordinates were obtained from RefSeq gene annotations downloaded from the UCSC genome browser. Reads were extended 100 bp to account for the size of the fragment isolated by the ChIP reaction. Integrated profiles were created by averaging the observed signal for each bin for the selected set of relevant genes; values displayed indicate fragments per 50 bp bin per million mapped reads. Using a very restrictive false discovery rate (FDR) = 5% as a cutoff and a significance score (fold-change score over input) of 2, we identified 9471 genes, and 15052 genes for H3K27me3 and H3K4me3, respectively. An

FPKM cutoff of > 1.2 was applied to yield high H3K27me3 (2057) and H3K4me3 (10007) genes, which were also used to identify gene bivalency. Heatmap displays were generated by ordering all genes by the indicated ranking (gene expression/H3K27me3 enrichment) and generated with Java TreeView. FPKM values were computed by calculating the number of reads per million per kb with respect to the TSS coordinates of RefSeq transcript. A pseudocount of one read per 25 million mapped reads was added to avoid division by zero errors. Values were rank-ordered and used for iPAGE analysis. iPAGE analysis was performed as described in Goodarzi et al.[60]. Briefly, genes are organized into even-numbered bins based on specific criteria; in this case genes were rank ordered according to H3K27me3 enrichment with respect to the TSS. Each bin and its neighboring bins are assessed for over/under-representation of ontology terms. This approach allows for the simultaneous display of specific terms or pathways that are over or under-represented in either of both, high or low ranking transcripts. Gene ontology was analyzed using the online DAVID gene ontology program specifying for biological processes. P-values of representative GO categories are displayed in bar graphs.

Sequential ChIP

Cross-linked and sorted chromatin from adult *ex vivo* isolated MSN nuclei (6×10^6 nuclei for each ChIP) was immunoprecipitated with antibody against H3K27me3 followed by immunoprecipitation with antibody against H3K4me3 using the Re-ChIP-IT sequential ChIP kit from Active Motif (cat# 53016) following manufacturers recommendations. The eluted chromatin was extracted and purified as described above (see “Chromatin Immunoprecipitation”). In addition, a control sequential ChIP was carried out in which chromatin was immunoprecipitated first with antibody against H3K27me3 followed by antibody against IgG.

Real-Time sequential ChIP-PCR

Primers to evaluate sequential ChIP assays were designed using Primer3 software to amplify 100-150 bp fragments from the indicated genomic regions. Real-time PCR was carried out using SYBR green PCR mix (Invitrogen) on an Applied Biosystems Step One Plus instrument. Serial dilutions of input material were used to determine standard curves for each individual primer pair. For sequential ChIP experiments, 2 ul sequential ChIP DNA was used as a template, and fold-enrichments were calculated over the second ChIP IgG control. Enrichments were determined from three independent sequential ChIP experiments, each evaluated in duplicates by real-time PCR. Primer sequences used were the following:

Eomes: forward GCAGGGAGCTTGTAAAGACG, reverse TTTGAAGTCTGCGAACATGG

Pmaip1: forward CAGGGCTTCTACCGAGACTG, reverse CCCACGAATCAGACGAGAAT

Pou4f1: forward CGGGACTGCTCTTAGAGGGA, reverse AAGTGGAGCCAAGTCGACAG

Gapdh: forward ACCGAAGAACAACGAGGAGA, reverse GAGACCTGAATGCTGCTTCC

Gip: forward CTGTGCCCAGGAAAGAAGAG, reverse GGCTGTGCTAATGGGTGATT

RNA isolation and preparation

RNA was prepared as previously described[61]. Briefly, mice were anesthetized with CO_2 followed by decapitation. Brain regions of interest were rapidly dissected and frozen in liquid nitrogen and stored at -80 °C until further processing. RNA extraction from frozen samples was performed using the TRIzol/Chloroform technique according to the manufacturer's instructions (Invitrogen Corporation, Carlsbad, CA). After extraction, RNA was precipitated overnight at -80 °C in isopropanol with 0.15M sodium acetate, washed twice with 70% ethanol, air-dried, and resuspended in nucelase-free water. RNase-free DNase treatment was performed using an RNeasy micro kit (Qiagen, Valencia, CA as previously described[62].

Quantitative qRT-PCR analysis

cDNA was prepared from DNase-treated total RNA using the High Capactiy RNA-to-cDNA kit (Applied Biosystems). Relative gene expression of the cDNA was assayed by qRT-PCR using pre-designed recommended Taqman gene expression assays from Applied Biosystems (ABI) following manufacturer's recommendations. Cycle counts for mRNA quantification were normalized to Actb or Gapdh. Relative expression (ΔCt) and quantification (RQ=2-ΔΔC) for each mRNA were calculated using ΔΔCt method as suggested.

Microarray gene expression analysis

Trizol-Chloroform extracted and RNeasy Micro Kit purified RNA was amplified and processed according to the Affymetrix cDNA synthesis kit. For all experiments, Affymetrix Mouse Genome 430 2.0 arrays were used. A GeneChIP Scanner 3000 (Affymetrix, Santa Clara, CA) was used to scan Mouse Genome 430 2.0 arrays. Arrays were globally scaled to 150 by the Affymetrix GeneChip operating software (GCOS CA). A differential expression of $P < 0.05$, moderated *t*-Test (genotype) was used to determine whether a gene was significantly changed. Gene expression changes are displayed in volcano plots where the corrected p-value (-log10) is plotted against the fold change (log2).

TRAP analysis

TRAP-based purification of ribosome associated mRNA from control and Ezh1 and Ezh2 deficient D1 MSNs (*Ezh1*$^{-/-}$*; Ezh2*$^{fl/fl}$*; Drd1a-cre; Drd1-TRAP* and control *Ezh1*$^{+/-}$*; Ezh2*$^{fl/fl}$*; Drd1-TRAP*), D2 MSN (*Drd2-cre; Ezh1*$^{-/-}$*; Ezh2*$^{fl/fl}$*; Drd2-Cre; Drd2-TRAP* and *Ezh1*$^{+/-}$*; Ezh2*$^{fl/fl}$*; Drd2-TRAP* mice) and cerebellar Purkinje cells (*Ezh1*$^{-/-}$*; Ezh2*$^{fl/fl}$*; Pcp2-Cre; Pcp2-TRAP* and control *Ezh1*$^{+/-}$*; Ezh2*$^{fl/fl}$*; Pcp2-TRAP* mice) was performed as previously described[23,62] ($n = 3$ each).

Gene expression as a function of histone methylation status

Genes were segregated into different histone methylation groups: H3K4me3 positive, H3K27me3 positive, H3K4me3/H3K27me3 positive or “None” groups based on ChIP-Seq experiments described above. Each gene in these gene sets was annotated with the average

FPKM from D1/D2 MSNs (n = 2 per group) and plotted in the Tukey box-plot format to display the median and variance of each gene group. A One-Way Anova was used to determine significance.

Transcription factor binding prediction

The presence of conserved cis-regulatory DNA elements in PRC2 target genes was analyzed using Genomatix[63] and oPOSSUM software[64]. Vertebrate-specific position specific scoring matrices (PSSMs) catalogued by JASPAR[65] were used to identify relationships between transcription factor binding sites (TFBS) and their target DNA binding motifs, restricting the search space for TFBS to phylogenetically conserved, non-coding DNA to improve specificity[66,67].

Gene list enrichment analysis

Gene list enrichment analysis was performed for significantly up-regulated genes 3 months and 6 months after PRC2 deletion using Enrichr[68,69]. Canvas layout was used to visualize enriched gene sets. Enriched terms are highlighted in color where the brightness indicates a lower p-value[70]; the closeness of tiles corresponds to similarities among gene sets and the brightness corresponds to the significance of enrichment between the input gene list and gene sets in the gene set libraries. P-values were calculated using a modified Hypergeometric Test with Benjamini-Hochberg correction.

Construction of transcription factor (TF) target networks

To construct the TF-target networks, we first collected TF target connections from ChIP-sequencing experiments performed in mice from ChEA[71] and ENCODE[72] to form a background TF target network in mice. We then seeded the up-regulated genes in the background network and kept only the direct TF target edges among the up-regulated genes. Cytoscape was used to generate the force-directed layout of the networks.

Protein preparation and Western blot analysis

Tissue—Mice were anesthetized with CO_2 followed by decapitation, and the cortex, hippocampus, striatum and cerebellum were rapidly dissected and frozen in liquid nitrogen and stored at -80 °C until further processing. Samples were sonicated at 4 °C in 1% SDS solution supplemented with protease inhibitor (Roche, Switzerland) and *PhosStop* phosphatase inhibitor (Roche, Switzerland), and boiled for ten minutes. The protein concentration was determined using a BCA protein assay kit (ThermoFisherScientific, USA) according to the manufacturer's instructions. Protein samples were diluted in equal volume of 2X LDS sample buffer (Invitrogen) and supplemented with DTT to a final concentration of 200 mM (Sigma).

Nuclei—Pelleted neuronal and glial nuclei fractions containing 100,000 nuclei each obtained from FACS (see *Purification of cell-type specific nuclei from mouse brain* above) were resuspended in 1X LDS sample buffer (Invitrogen) supplemented with 1% SDS and DTT (200 mM, Sigma). Nuclei resuspensions were sonicated in a Bioruptor on high power

in 30 s On/30 s Off cycles for a total of 10 cycles at 4 °C. Samples were then boiled for ten minutes.

20 μg of protein samples or complete lysate from 100,000 nuclei were separated on 4-12% Bolt Bis-tris precast denaturing gels (Invitrogen, USA) and transferred onto PVDF membranes. Membranes were probed with primary antibodies diluted in 5% milk-TBST solution overnight at 4 °C. Membranes were then washed and probed with horseradish-peroxidase conjugated anti-mouse (GE), anti-rabbit IgG secondary antibody (GE), or anti-goat IgG antibody (Jackson Immunoresearch, USA) for one hour at room temperature. Membranes were developed using enhanced chemiluminescence substrate (PerkinElmer, USA) and exposed on film. Exposed films were scanned, and protein bands were quantified using ImageJ Software (NIH, USA). Protein quantities were normalized using beta-Actin, Gapdh or β III Neuron specific tubulin. All values were plotted relative to control littermate sample. Primary antibodies used see Supplementary Table 8.

Slice preparation and single molecule *in situ* hybridization

Mice were anesthetized with Ketamine (120 mg/kg) and Xylazine (24 mg/kg) and perfused transcardially with 50 ml PBS, followed by removal and fixation of the brain in 10% neutral-buffered formalin. Fixed brains were imbedded in paraffin and sliced in 5 μm-thick section. *In situ* hybridization was carried out using RNAScope custom designed probes for *Barx1, Drd2, Nkx2-5, Pitx2, Pou4f1, Sfmbt2, Tal1, Twist1* and *Zic2* in combination with the RNAScope 2.0 Red kit following manufacturer's recommendation (Advanced Cell Diagnostics). After completing *in situ* hybridization, sections were stained with DAPI (0.2 mg/ml), imaged on the Zeiss LSM 780 confocal microscope and analyzed using the Zen 2011 software. Cell counting was done using Image J's cell counter tool. Drd2 intensities were measured by marking the cell area and measuring the mean fluorescence intensity inside the area.

Immunofluorescence

Mice were anesthetized with Ketamine (120 mg/kg) and Xylazine (24 mg/kg) and perfused transcardially with 10 ml PBS and 40 ml 4% paraformaldehyde (Electron microscopy sciences) as previously described[62]. Fixed brains were removed and dehydrated in 5%, 15% and 30% sucrose in PBS. Following dehydration, brains were frozen in Neg-50 (Thermo Scientific) on dry ice and stored at -80 °C until further processing. Brains were cut using a cryostat and 12-18um sections were mounted on superfrost plus microscope slides (Fisher Scientific). Slides were stored at -80 °C until staining. Slides were washed with PBS, permeabilized with PBS + 0.2% Tritonx-100 and incubated with Image-iT FX Signal enhancer (Invitrogen) followed by blocking with 2% Normal Goat Serum in PBS + 0.2% Tritonx-100. Slides were incubated with primary antibody (see Supplementary Table 8) in 2% Normal Goat Serum in PBS + 0.2% Tritonx-100 overnight at 4 °C. Slides were then washed and incubated with Alexa Fluor conjugated secondary antibodies (Alexa Fluor 488 and 568 labeled goat anti-mouse or anti-rabbit IgGs (H+L); see Supplementary Table 8) in 2% Normal Goat Serum in PBS + 0.2% Tritonx-100 for one hour at room temperature. Slides were washed and cover-slipped using Prolong-gold anti-fade with DAPI (Invitrogen). Image processing was performed using the Zeiss LSM 780 confocal microscope and Zen

2011 software. Immunofluorescent images were analyzed using the Image J software. The diameter of the cerebellar lobe folds were measured and analyzed in Image J.

Nissl Staining

Brain sections were permeabilized in phosphate-buffered saline (PBS) with 0.1% Triton X-100 (PBS-T) for ten minutes at room temperature followed by washes in PBS. Sections were incubated in NeuroTrace 530/615 (Life Technologies, cat# N21482) (1:200 in PBS) for twenty minutes at room temperature and washed once with PBS-T and twice with PBS. DAPI (1:10,000 in PBS) was added for 15 minutes, followed by three PBS washes. Sections were mounted using Prolong Gold mounting media.

Electron Microscopy

Mice were anesthetized with Ketamine (120 mg/kg) and Xylazine (24 mg/kg) and sacrificed by intracardiac perfusion with 0.1 M sodium cacodylate buffer (pH 7.4) followed by the fixative, which contained 2.5% glutaraldehyde and 2% paraformaldehyde in the buffer. After removal from the skull, the brains were post-fixed in the fresh fixative overnight at 4 °C and sliced by a vibrating blade microtome (VT100S, Leica microsystem, Buffalo Grove, IL) at 50 μm thickness. Subsequently, they underwent post-fixation in 1% osmium tetroxide for one hour, *en block* staining with 0.5% Uranyl acetate for 30 min, dehydration with a graded series of ethanol, and infiltration/embedding in EMBed812 resin. A slice was prepared from striatum at the level of 0.8-0.9mm from Bregma and it was divided into four areas, including dorsolateral (DL), dorsomedial (DM), ventrolateral (VL) and ventromedial (VM). DL and VM were selected as the regions of analysis based on the preliminary observation. Ultrathin sections were cut and thoroughly examined in the electron microscope (100CX JEOL, Tokyo, Japan) with the digital imaging system (XR41-C, Advantage Microscopy Technology Corp, Denver, MA).

Behavioral analysis

All behavior analyses (excluding the 24-hour observation) were performed during the 0700-1900 light cycle as previously described[61,62,73]. For all behavioral experiments, experimenters were blinded to the genotypes of the animals. Genotypes were decoded after data was processed and analyzed. Subjects corresponding to data points that are more than 2 standard deviations from the sample mean were excluded from analyses. When possible, all littermate animals were included in behavioral experiments as control groups. No randomization protocol was used. Animals were allocated to treatment groups to ensure uniform distribution of ages and sexes in each group. Where 2 conditions are compared, a two-tailed unpaired Student's *t* test was used. All procedures were conducted in strict accordance with the National Institutes of Health Guide for the Care and Use of Laboratory Animals and were approved by the IACUC at Icahn School of Medicine at Mount Sinai.

Open-Field analysis—Locomotion and exploratory behavior was analyzed by open field analysis as previously described[62].

Rotarod analysis—Balance and motor function of mice was measured using the standard accelerated Rota rod test (Med Associates, St. Albans, VT) with a rotation speed of 4-40 rpms within 5 minutes. Scoring and analysis was carried out as in Schaefer et al., 2009[62].

Hanging Wire analysis—The ability of mice to hang onto a wire lid was measured by the Hanging Wire test[74]. Briefly, mice were placed on a standard wire cage lid, and the lid was lightly shaken to ensure a tight grip of the mice to the wire. The wires lids were turned upside down and held approximately 20 cm over the home cage for 60 seconds. Latency to fall off the wire lid was measured.

Footprint pattern analysis—Footprint pattern was analyzed as previously described[74]. The hind and forefeet were dipped into non-toxic paint (hind feet black, forefeet red). Mice were allowed to walk through a 9 cm wide, 35 cm long and 6 cm high tunnel lined with white paper, and the resulting footprint pattern was analyzed.

Survival curve—Date of death in the home cage for mutants and control littermates was recorded and plotted as Kaplan-Meier survival curve.

Electrophysiology

All recordings were carried out blind to the experimental conditions of the mice. Whole-cell recordings were obtained from anterior dorsolateral-striatum medium spiny neurons (MSNs) in acute brain slices from 4-month old age-matched *Ezh1*$^{-/-}$*; Ezh2*$^{fl/fl}$*; Camk2a-cre mice* and their respective littermate controls. Acute brain slices were prepared as described previously[55,75,76]. To minimize possible stress and to obtain healthy striatum slices, mice were anesthetized and perfused immediately for 40-60 s with ice-cold artificial cerebrospinal fluid (aCSF), which contained 128 mM NaCl, 3 mM KCl, 1.25 mM NaH_2PO_4, 10 mM D-glucose, 24 mM $NaHCO_3$, 2 mM $CaCl_2$ and 2 mM $MgCl_2$ (oxygenated with 95% O_2 and 5% CO_2, pH 7.35, 295-305 mOsm). Acute brain slices (250 μm) containing striatum were cut using a microslicer (DTK-1000, Ted Pella) in sucrose-ACSF, which was derived by fully replacing NaCl with 254 mM sucrose, and saturated by 95% O_2 and 5% CO_2. Slices were maintained in the holding chamber for one hour recovery at 37° C, and then were kept at room temperature for recordings. Slices were transferred into a recording chamber with a constant flow rate of aCSF equilibrated with 95% O_2 and 5% CO_2 (flow rate = 2.5 ml min^{-1}) at 35 °C.

Whole-cell current-clamp recordings were carried out as described previously[55,75,76]. Glass microelectrodes (3-5 MΩ) were filled with an internal solution containing 115 mM potassium gluconate, 20 mM KCl, 1.5 mM $MgCl_2$, 10 mM phosphocreatine, 10 mM HEPES, 2 mM magnesium ATP and 0.5 mM GTP (pH 7.2, 285 mOsm). To measure the intrinsic membrane properties of striatum MSNs, whole-cell recordings were made under the current-clamp configuration (Multiclamp 700B, Axon Instruments). Data acquisition was made using Digidata 1440A and pClamp10 (Molecular Devices). Series resistance was monitored during all recordings. For all measurements of neuronal excitability, a current was injected in 0.8 s increments as previously described (step, 50 pA; range, -50 to 400 pA) in current-clamp mode[55]. Rheobase (first spike induced by current injection) was measured

following neuronal excitability recording. To measure input resistance (current-voltage relationship), a current was injected in 0.4 s increments as previously described (steps, 25pA; range, 50 to -200 pA)[55].

Statistical analysis

Statistics were analyzed using GraphPad Prism v5.01and significance was determined at $P < 0.05$. All statistical analyses were two-tailed. All data was normally distributed as assessed by the Kolmogorov-Smirnov (K-S) test. For two group comparisons with equal variance as determined by the F test, an unpaired student *t* test was used. Welch's correction was used for an unpaired *t*-test of normally distributed data with unequal variance. For multiple group comparisons, either One-Way or Two-Way ANOVA with repeated measures was used. Error bars display SEM. Significance of venn diagrams was calculated using the non-parametric analysis Chi-square test. No statistical methods were used to predetermine the sample size, but our sample sizes are similar to those generally employed in the field.

Data availability

ChIP-sequencing and microarray data sets have been deposited in the GEO database at NCBI. All data sets for this study are available under GSE84245. Original western blot scans are shown in Supplementary Figure 9 and 10. Gene ontology data are available in Supplementary Tables 2, 3 and 6. All data that support the findings of this study are available from the corresponding author upon request. Statistical analyses for all experiments are detailed in the figure legends and in the Supplementary methods checklist with complete statistical details of all experiments.

Supplementary Material

Refer to Web version on PubMed Central for supplementary material.

Acknowledgments

We would like to thank P. Greengard for helpful discussions, T. Jenuwein from the MPI in Freiburg for providing the Ezh1$^{-/-}$ mice, N. Heintz from the Rockefeller University for providing the Pcp2-TRAP mice, K. Uryu for electron microscopy, Joe Scarpa and Fan Zhang for their assistance with the bio-informatics analyses, and S. Mann and S. Kalik for technical assistance and animal work. This work was supported by the National Institutes of Health (NIH) Director New Innovator Award DP2 MH100012-01 (A. Schaefer), 1R01NS091574 (A. Schaefer), CURE Challenge Award (A. Schaefer), 5R01GM112811 (A. Tarakhovsky), the Emerald Foundation Inc.(A. Tarakhovsky), NARSAD Young Investigator Award #22802 (M. v. Schimmelmann), T32AG049688 (A. Badimon), 5T32MH096678 (J.M. Sullivan), 1RO1MH092306 (M.H. Han), J&J/IMHRO Translational Research Star Award (M.H. Han), NARSAD Independent Investigator Award (M.H. Han), 1 F31MH108326 (S.M. Ku), R01GM098316 (A. Ma'ayan), U54HG008230 (A. Ma'ayan), and U54CA189201 (A. Ma'ayan),.

References

1. Hobert O. Regulation of terminal differentiation programs in the nervous system. Annual review of cell and developmental biology. 2011; 27:681–696. DOI: 10.1146/annurev-cellbio-092910-154226
2. Molyneaux BJ, Arlotta P, Menezes JR, Macklis JD. Neuronal subtype specification in the cerebral cortex. Nature reviews Neuroscience. 2007; 8:427–437. DOI: 10.1038/nrn2151 [PubMed: 17514196]
3. Deneris ES, Hobert O. Maintenance of postmitotic neuronal cell identity. Nature neuroscience. 2014; 17:899–907. DOI: 10.1038/nn.3731 [PubMed: 24929660]

4. Corley M, Kroll KL. The roles and regulation of Polycomb complexes in neural development. Cell and tissue research. 2015; 359:65–85. DOI: 10.1007/s00441-014-2011-9 [PubMed: 25367430]
5. Margueron R, et al. Ezh1 and Ezh2 maintain repressive chromatin through different mechanisms. Molecular cell. 2008; 32:503–518. DOI: 10.1016/j.molcel.2008.11.004 [PubMed: 19026781]
6. Margueron R, Reinberg D. The Polycomb complex PRC2 and its mark in life. Nature. 2011; 469:343–349. DOI: 10.1038/nature09784 [PubMed: 21248841]
7. Laible G, et al. Mammalian homologues of the Polycomb-group gene Enhancer of zeste mediate gene silencing in Drosophila heterochromatin and at S. cerevisiae telomeres. The EMBO journal. 1997; 16:3219–3232. DOI: 10.1093/emboj/16.11.3219 [PubMed: 9214638]
8. Swigut T, Wysocka J. H3K27. demethylases, at long last. Cell. 2007; 131:29–32. DOI: 10.1016/j.cell.2007.09.026 [PubMed: 17923085]
9. He XB, et al. Vitamin C facilitates dopamine neuron differentiation in fetal midbrain through TET1- and JMJD3-dependent epigenetic control manner. Stem Cells. 2015; 33:1320–1332. DOI: 10.1002/stem.1932 [PubMed: 25535150]
10. Palomer E, Carretero J, Benvegnu S, Dotti CG, Martin MG. Neuronal activity controls Bdnf expression via Polycomb de-repression and CREB/CBP/JMJD3 activation in mature neurons. Nature communications. 2016; 7:11081.
11. Li J, et al. EZH2-mediated H3K27 trimethylation mediates neurodegeneration in ataxia-telangiectasia. Nature neuroscience. 2013; 16:1745–1753. DOI: 10.1038/nn.3564 [PubMed: 24162653]
12. Sodersten E, et al. Dopamine signaling leads to loss of Polycomb repression and aberrant gene activation in experimental parkinsonism. PLoS genetics. 2014; 10:e1004574. [PubMed: 25254549]
13. Seong IS, et al. Huntingtin facilitates polycomb repressive complex 2. Human molecular genetics. 2010; 19:573–583. DOI: 10.1093/hmg/ddp524 [PubMed: 19933700]
14. Dong X, et al. The Role of H3K4me3 in Transcriptional Regulation Is Altered in Huntington's Disease. PloS one. 2015; 10:e0144398. [PubMed: 26636336]
15. Biagioli M, et al. Htt CAG repeat expansion confers pleiotropic gains of mutant huntingtin function in chromatin regulation. Human molecular genetics. 2015; 24:2442–2457. DOI: 10.1093/hmg/ddv006 [PubMed: 25574027]
16. Hoss AG, et al. MicroRNAs located in the Hox gene clusters are implicated in huntington's disease pathogenesis. PLoS genetics. 2014; 10:e1004188. [PubMed: 24586208]
17. Labadorf A, et al. RNA Sequence Analysis of Human Huntington Disease Brain Reveals an Extensive Increase in Inflammatory and Developmental Gene Expression. PloS one. 2015; 10:e0143563. [PubMed: 26636579]
18. Su IH, et al. Polycomb group protein ezh2 controls actin polymerization and cell signaling. Cell. 2005; 121:425–436. DOI: 10.1016/j.cell.2005.02.029 [PubMed: 15882624]
19. Santos-Rosa H, et al. Active genes are tri-methylated at K4 of histone H3. Nature. 2002; 419:407–411. DOI: 10.1038/nature01080 [PubMed: 12353038]
20. Voigt P, Tee WW, Reinberg D. A double take on bivalent promoters. Genes & development. 2013; 27:1318–1338. DOI: 10.1101/gad.219626.113 [PubMed: 23788621]
21. Bernstein BE, et al. A bivalent chromatin structure marks key developmental genes in embryonic stem cells. Cell. 2006; 125:315–326. DOI: 10.1016/j.cell.2006.02.041 [PubMed: 16630819]
22. Ku M, et al. Genomewide analysis of PRC1 and PRC2 occupancy identifies two classes of bivalent domains. PLoS genetics. 2008; 4:e1000242. [PubMed: 18974828]
23. Heiman M, et al. A translational profiling approach for the molecular characterization of CNS cell types. Cell. 2008; 135:738–748. DOI: 10.1016/j.cell.2008.10.028 [PubMed: 19013281]
24. Lein ES, et al. Genome-wide atlas of gene expression in the adult mouse brain. Nature. 2007; 445:168–176. DOI: 10.1038/nature05453 [PubMed: 17151600]
25. Hersch SM, et al. Electron microscopic analysis of D1 and D2 dopamine receptor proteins in the dorsal striatum and their synaptic relationships with motor corticostriatal afferents. The Journal of neuroscience : the official journal of the Society for Neuroscience. 1995; 15:5222–5237. [PubMed: 7623147]

26. Fridman JS, Lowe SW. Control of apoptosis by p53. Oncogene. 2003; 22:9030–9040. DOI: 10.1038/sj.onc.1207116 [PubMed: 14663481]
27. Kranenburg O, van der Eb AJ, Zantema A. Cyclin D1 is an essential mediator of apoptotic neuronal cell death. The EMBO journal. 1996; 15:46–54. [PubMed: 8598205]
28. Marathe S, Liu S, Brai E, Kaczarowski M, Alberi L. Notch signaling in response to excitotoxicity induces neurodegeneration via erroneous cell cycle reentry. Cell death and differentiation. 2015; 22:1775–1784. DOI: 10.1038/cdd.2015.23 [PubMed: 25822340]
29. Lovell MA, Xie C, Xiong S, Markesbery WR. Wilms' tumor suppressor (WT1) is a mediator of neuronal degeneration associated with the pathogenesis of Alzheimer's disease. Brain research. 2003; 983:84–96. [PubMed: 12914969]
30. Lu XH, et al. Targeting ATM ameliorates mutant Huntingtin toxicity in cell and animal models of Huntington's disease. Science translational medicine. 2014; 6:268ra178.
31. Illuzzi J, Yerkes S, Parekh-Olmedo H, Kmiec EB. DNA breakage and induction of DNA damage response proteins precede the appearance of visible mutant huntingtin aggregates. Journal of neuroscience research. 2009; 87:733–747. DOI: 10.1002/jnr.21881 [PubMed: 18831068]
32. Anne SL, Saudou F, Humbert S. Phosphorylation of huntingtin by cyclin-dependent kinase 5 is induced by DNA damage and regulates wild-type and mutant huntingtin toxicity in neurons. The Journal of neuroscience : the official journal of the Society for Neuroscience. 2007; 27:7318–7328. DOI: 10.1523/JNEUROSCI.1831-07.2007 [PubMed: 17611284]
33. Turmaine M, et al. Nonapoptotic neurodegeneration in a transgenic mouse model of Huntington's disease. Proceedings of the National Academy of Sciences of the United States of America. 2000; 97:8093–8097. DOI: 10.1073/pnas.110078997 [PubMed: 10869421]
34. Orlando V. Polycomb, epigenomes, and control of cell identity. Cell. 2003; 112:599–606. [PubMed: 12628181]
35. Doyle JP, et al. Application of a translational profiling approach for the comparative analysis of CNS cell types. Cell. 2008; 135:749–762. DOI: 10.1016/j.cell.2008.10.029 [PubMed: 19013282]
36. Savas JN, Toyama BH, Xu T, Yates JR 3rd, Hetzer MW. Extremely long-lived nuclear pore proteins in the rat brain. Science. 2012; 335:942. [PubMed: 22300851]
37. Duerre JA, Lee CT. In vivo methylation and turnover of rat brain histones. Journal of neurochemistry. 1974; 23:541–547. [PubMed: 4421616]
38. Culhane JC, Cole PA. LSD 1 and the chemistry of histone demethylation. Current opinion in chemical biology. 2007; 11:561–568. DOI: 10.1016/j.cbpa.2007.07.014 [PubMed: 17851108]
39. Dobenecker MW, et al. Coupling of T cell receptor specificity to natural killer T cell development by bivalent histone H3 methylation. J Exp Med. 2015; 212:297–306. DOI: 10.1084/jem.20141499 [PubMed: 25687282]
40. Mohn F, et al. Lineage-specific polycomb targets and de novo DNA methylation define restriction and potential of neuronal progenitors. Molecular cell. 2008; 30:755–766. DOI: 10.1016/j.molcel.2008.05.007 [PubMed: 18514006]
41. Barski A, et al. High-resolution profiling of histone methylations in the human genome. Cell. 2007; 129:823–837. DOI: 10.1016/j.cell.2007.05.009 [PubMed: 17512414]
42. Wachter E, et al. Synthetic CpG islands reveal DNA sequence determinants of chromatin structure. eLife. 2014; 3:e03397. [PubMed: 25259796]
43. Mendenhall EM, et al. GC-rich sequence elements recruit PRC2 in mammalian ES cells. PLoS genetics. 2010; 6:e1001244. [PubMed: 21170310]
44. Kaneko S, Son J, Bonasio R, Shen SS, Reinberg D. Nascent RNA interaction keeps PRC2 activity poised and in check. Genes & development. 2014; 28:1983–1988. DOI: 10.1101/gad.247940.114 [PubMed: 25170018]
45. Jadhav U, et al. Acquired Tissue-Specific Promoter Bivalency Is a Basis for PRC2 Necessity in Adult Cells. Cell. 2016; 165:1389–1400. DOI: 10.1016/j.cell.2016.04.031 [PubMed: 27212235]
46. Langfelder P, et al. Integrated genomics and proteomics define huntingtin CAG length-dependent networks in mice. Nature neuroscience. 2016; 19:623–633. DOI: 10.1038/nn.4256 [PubMed: 26900923]

47. Vashishtha M, et al. Targeting H3K4 trimethylation in Huntington disease. Proceedings of the National Academy of Sciences of the United States of America. 2013; 110:E3027–3036. DOI: 10.1073/pnas.1311323110 [PubMed: 23872847]
48. Klapstein GJ, et al. Electrophysiological and morphological changes in striatal spiny neurons in R6/2 Huntington's disease transgenic mice. J Neurophysiol. 2001; 86:2667–2677. [PubMed: 11731527]
49. Menalled LB, Chesselet MF. Mouse models of Huntington's disease. Trends Pharmacol Sci. 2002; 23:32–39. [PubMed: 11804649]
50. Reynolds JP, et al. Transcriptional Response of Polycomb Group Genes to Status Epilepticus in Mice is Modified by Prior Exposure to Epileptic Preconditioning. Frontiers in neurology. 2015; 6:46. [PubMed: 25806020]
51. Casanova E, et al. A CamKIIalpha iCre BAC allows brain-specific gene inactivation. Genesis. 2001; 31:37–42. [PubMed: 11668676]
52. Schaefer A, et al. Cerebellar neurodegeneration in the absence of microRNAs. J Exp Med. 2007; 204:1553–1558. DOI: 10.1084/jem.20070823 [PubMed: 17606634]
53. Zhang XM, et al. Highly restricted expression of Cre recombinase in cerebellar Purkinje cells. Genesis. 2004; 40:45–51. DOI: 10.1002/gene.20062 [PubMed: 15354293]
54. Ezhkova E, et al. EZH1 and EZH2 cogovern histone H3K27 trimethylation and are essential for hair follicle homeostasis and wound repair. Genes & development. 2011; 25:485–498. DOI: 10.1101/gad.2019811 [PubMed: 21317239]
55. Maze I, et al. G9a influences neuronal subtype specification in striatum. Nature neuroscience. 2014; 17:533–539. DOI: 10.1038/nn.3670 [PubMed: 24584053]
56. Maze I, et al. Essential role of the histone methyltransferase G9a in cocaine-induced plasticity. Science. 2010; 327:213–216. DOI: 10.1126/science.1179438 [PubMed: 20056891]
57. Kriaucionis S, Heintz N. The nuclear DNA base 5-hydroxymethylcytosine is present in Purkinje neurons and the brain. Science. 2009; 324:929–930. DOI: 10.1126/science.1169786 [PubMed: 19372393]
58. Gao Z, et al. An AUTS2-Polycomb complex activates gene expression in the CNS. Nature. 2014; 516:349–354. DOI: 10.1038/nature13921 [PubMed: 25519132]
59. Mullen RJ, Buck CR, Smith AM. NeuN, a neuronal specific nuclear protein in vertebrates. Development. 1992; 116:201–211. [PubMed: 1483388]
60. Goodarzi H, Elemento O, Tavazoie S. Revealing global regulatory perturbations across human cancers. Molecular cell. 2009; 36:900–911. DOI: 10.1016/j.molcel.2009.11.016 [PubMed: 20005852]
61. Tan CL, et al. MicroRNA-128 governs neuronal excitability and motor behavior in mice. Science. 2013; 342:1254–1258. DOI: 10.1126/science.1244193 [PubMed: 24311694]
62. Schaefer A, et al. Control of cognition and adaptive behavior by the GLP/G9a epigenetic suppressor complex. Neuron. 2009; 64:678–691. DOI: 10.1016/j.neuron.2009.11.019 [PubMed: 20005824]
63. Cartharius K, et al. MatInspector and beyond: promoter analysis based on transcription factor binding sites. Bioinformatics. 2005; 21:2933–2942. DOI: 10.1093/bioinformatics/bti473 [PubMed: 15860560]
64. Kwon AT, Arenillas DJ, Worsley Hunt R, Wasserman WW. oPOSSUM-3: advanced analysis of regulatory motif over-representation across genes or ChIP-Seq datasets. G3 (Bethesda). 2012; 2:987–1002. DOI: 10.1534/g3.112.003202 [PubMed: 22973536]
65. Sandelin A, Alkema W, Engstrom P, Wasserman WW, Lenhard B. JASPAR: an open-access database for eukaryotic transcription factor binding profiles. Nucleic acids research. 2004; 32:D91–94. DOI: 10.1093/nar/gkh012 [PubMed: 14681366]
66. Dermitzakis ET, Clark AG. Evolution of transcription factor binding sites in Mammalian gene regulatory regions: conservation and turnover. Mol Biol Evol. 2002; 19:1114–1121. [PubMed: 12082130]
67. Lenhard B, et al. Identification of conserved regulatory elements by comparative genome analysis. J Biol. 2003; 2:13. [PubMed: 12760745]

68. Chen EY, et al. Enrichr: interactive and collaborative HTML5 gene list enrichment analysis tool. BMC bioinformatics. 2013; 14:128. [PubMed: 23586463]
69. Kuleshov MV, et al. Enrichr: a comprehensive gene set enrichment analysis web server 2016 update. Nucleic acids research. 2016
70. Tan CM, Chen EY, Dannenfelser R, Clark NR, Ma'ayan A. Network2Canvas: network visualization on a canvas with enrichment analysis. Bioinformatics. 2013; 29:1872–1878. DOI: 10.1093/bioinformatics/btt319 [PubMed: 23749960]
71. Lachmann A, et al. ChEA: transcription factor regulation inferred from integrating genome-wide ChIP-X experiments. Bioinformatics. 2010; 26:2438–2444. DOI: 10.1093/bioinformatics/btq466 [PubMed: 20709693]
72. An integrated encyclopedia of DNA elements in the human genome. Nature. 2012; 489:57–74. DOI: 10.1038/nature11247 [PubMed: 22955616]
73. Sullivan JM, et al. Autism-like syndrome is induced by pharmacological suppression of BET proteins in young mice. J Exp Med. 2015; 212:1771–1781. DOI: 10.1084/jem.20151271 [PubMed: 26392221]
74. Crawley, JN. What's wrong with my mouse? : behavioral phenotyping of transgenic and knockout mice. 2nd. Wiley-Interscience; 2007.
75. Lobo MK, et al. Cell type-specific loss of BDNF signaling mimics optogenetic control of cocaine reward. Science. 2010; 330:385–390. DOI: 10.1126/science.1188472 [PubMed: 20947769]
76. Wallace DL, et al. CREB regulation of nucleus accumbens excitability mediates social isolation-induced behavioral deficits. Nature neuroscience. 2009; 12:200–209. DOI: 10.1038/nn.2257 [PubMed: 19151710]

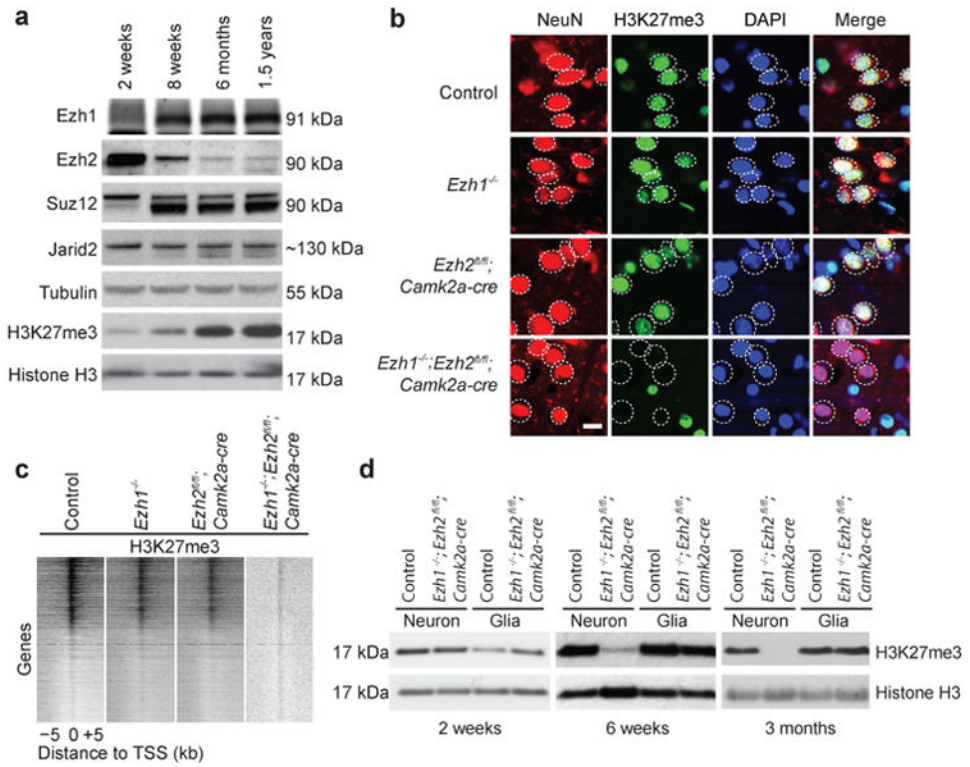

Fig. 1. Combined Ezh1 and Ezh2 deficiencies lead to H3K27me3 deficiency in adult neurons

(**a**) The expression levels of the indicated PRC2 components and H3K27me3 methylation were measured by Western blot analysis of striatal protein lysates derived from wild type C57BL/6J mice at indicated animal ages. Tubulin and histone H3 were used as loading controls. A representative image is shown (experiment was performed twice). **(b)** The expression of H3K27me3 (green) in the nucleus (DAPI, blue) of control or mutant MSNs (NeuN, red) were determined by immunofluorescence analysis of brain sections. Scale bar, 5 μm. A representative image is shown, n =3 mice per genotype. **(c)** The abundance of H3K27me3 at individual genes was determined by ChIP sequencing of chromatin derived from *ex vivo* purified MSN nuclei of wild type or mutant mice (n = 10 mice per genotype) and is displayed as a heat map over the transcriptional start site (TSS) +/-5kb (experiment was performed twice). **(d)** Age-dependent gradual loss of H3K27me3 in the striatum of *Ezh1*$^{-/-}$; *Ezh2*$^{fl/fl}$; *Camk2a-cre* mice. H3K27me3 methylation was measured by Western blot analysis of protein extracts derived from purified MSN or glia nuclei (100,000 per sample) of wild type or mutant mice (experiment was performed twice) at the indicated animal ages. Histone H3 was used as loading control.

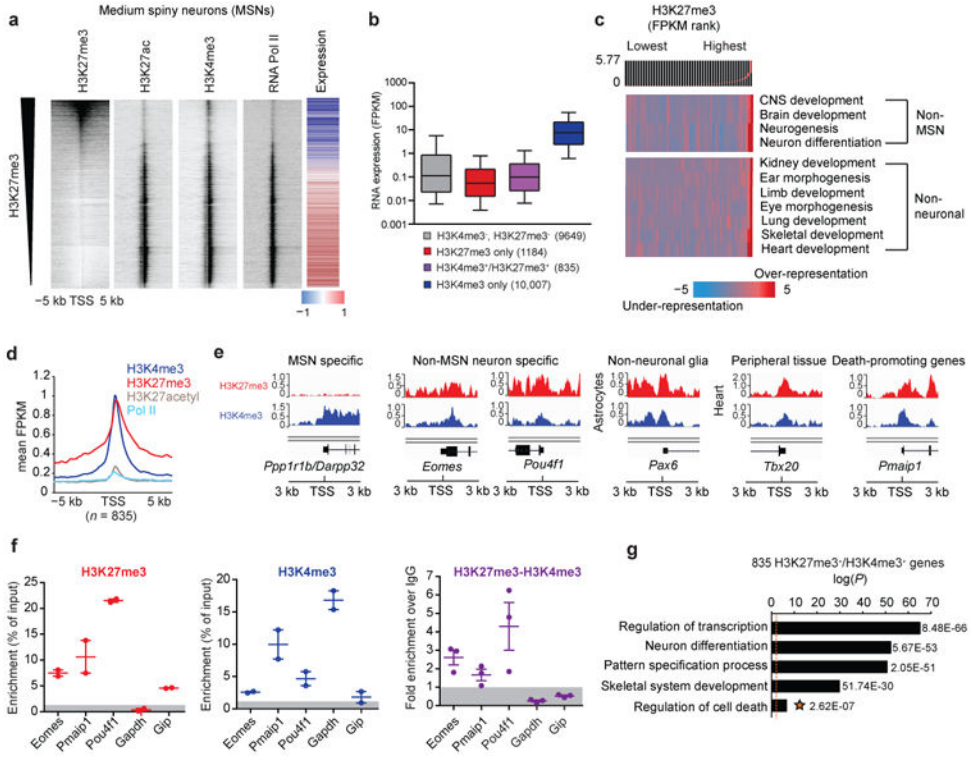

Fig. 2. H3K27me3 is associated with non-neuronal, non-medium spiny neuronal (MSN) and death promoting genes in adult MSNs

(**a**) The heat map shows the abundance of H3K27me3, H3K27acetyl, H3K4me3 and RNA Polymerase II at the TSS of individual genes in *ex vivo* isolated adult MSN nuclei (n = 10 mice per modification). Genes were ranked by H3K27me3 abundance. The MSN-specific mRNA expression levels correlate inversely with the H3K27me3 abundance. **(b)** H3K27me3 associated genes are not expressed in MSNs. Box plots display the median and variance of MSN specific gene expression levels (FPKM) of each indicated gene group, whiskers show 10th and 90th percentiles. (**c**) H3K27me3 associated genes in MSNs encode non-MSN expressed neuronal genes and non-neuronal genes. Categories of genes significantly enriched for H3K27me3 were determined by iPAGE analysis (Goodarzi et al., 2009; https://iget.c2b2.columbia.edu) and are grouped according to the indicated pathways. **(d)** The profile plot depicts mean H3K4me3, H3K27me3, H3K27acetyl, and Pol II coverage over the TSS (+/- 5kb) of 835 H3K27me3+/H3K4me3+ genes in MSNs. (**e**) Genome browser views show ChIP sequencing enrichment signals for H3K27me3 and H3K4me3 at the TSS (+/- 3kb) of the indicated genes (**f**) The amount of the chromatin-bound DNA immunoprecipitated with anti-H3K27me3 (left, red), anti-H3K4me3 (center, blue) antibodies, or following the sequential H3K27me3-H3K4me3 immunoprecipitation (right, purple) has been measured for three selected bivalent genes (*Eomes, Pmaip1, Pou4f1*) (experiment was performed three times), one H3K4me3 monovalent (*Gapdh*) (experiment was performed twice), and one H3K27me3 monovalent (*Gip*) gene (experiment was performed three times) by qPCR and is displayed as a percentage of the input for H3K27me3 and for H3K4me3, or as an enrichment over the IgG control in the second immunoprecipitation for the sequential ChIP. Data are mean ± SEM. (**g**) Gene ontology of

top-enriched biological pathways (-log10 p-value) of 835 H3K27me3+/H3K4me3+ genes is shown (David Gene Ontology Bioinformatic Resources, https://david.ncifcrf.gov/home.jsp). The dotted line indicates $P < 0.05$ from EASE Score, a modified Fisher Exact P-Value.

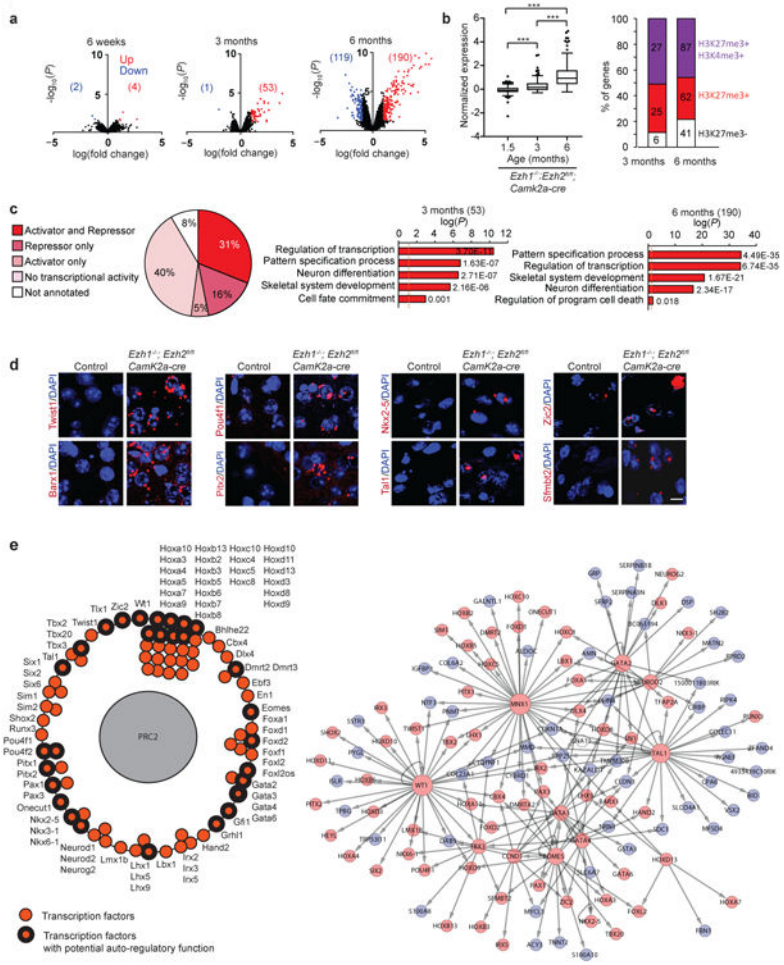

Fig. 3. Selective effect of PRC2 deficiency on MSN gene expression

(**a**) Volcano plots show changes in gene expression in PRC2 deficient neurons at 6 weeks, 3 and 6 months of age (6 weeks: $n = 3$ mice each (3 males each); 3 months: $n = 4$ control (2 males, 2 females), 3 mutant mice (1 male, 2 female mice); 6 months: $n = 4$ control (1 male, 3 females), 6 mutant mice; (2 males, 4 females)) ($P < 0.05$, fold change > 2). (**b**) (Left panel) The box plot shows the normalized expression values of 190 up-regulated genes at the indicated ages. $P < 0.0001$, F (2, 930) = 241 from one-way ANOVA with Tukey multiple comparison post- hoc analysis, whiskers show 10th and 90th percentiles. (Right panel) The bar diagram shows the percentage of the 53 and 190 up-regulated genes associated with H3K27me3/H3K4me3 (violet), H3K27me3 only (red), or none (white) in wild type MSNs. (**c**) Genes encoding transcriptional regulators are enriched among genes up-regulated in PRC2-deficient MSNs. The pie chart shows the percentage of genes in each category. Selected GO pathway annotation of up-regulated genes (-log10 p-value) at 3 and 6 month of age (David Gene Ontology Bioinformatic Resources, https://david.ncifcrf.gov/home.jsp) are shown, dotted line indicates $P < 0.05$ from EASE Score, a modified Fisher Exact P-Value. **(d)** Ectopic expression of non-neuronal and non-MSN expressed transcriptional regulators in PRC2-deficient MSNs was determined by *in situ* mRNA analysis (scale bar, 10 μm). Representative images of three independent experiments are shown. (**e**) (Left panel)

Graphical representation of transcription factors (TF, red circles) up-regulated in PRC2-deficient MSNs. The TFs that display potential auto-regulatory function are indicated (n= 29, black lined red circles). (Right panel) Up-regulated genes in PRC2-deficient MSNs form auto-/co-regulatory transcriptional networks. The networks connecting the genes up-regulated in PRC2-deficient MSNs at 6 month of age are based on experimental evidence from published ChIP-sequencing datasets from ChEA and ENCODE. Only studies in mice were included. TFs are colored in pink, non-TF genes are colored in blue. Nodes with outgoing links have evidence from ChIP-sequencing data. The size of the nodes is proportional to their connectivity degree.

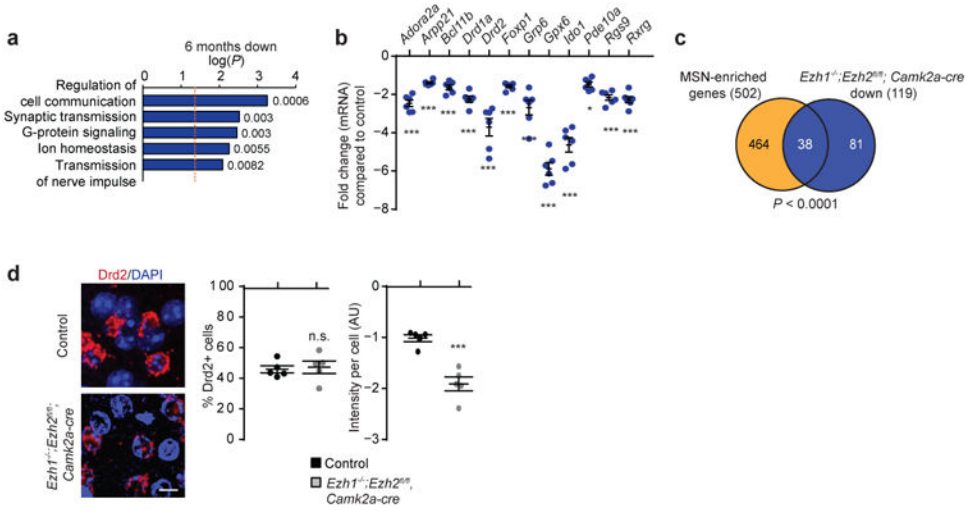

Fig. 4. PRC2 deficiency leads to the downregulation of MSN specific genes

(a) Selected GO pathways of down-regulated genes (-log10 p-value) are shown (David Gene Ontology Bioinformatic Resources, https://david.ncifcrf.gov/home.jsp). The dotted line indicates $P < 0.05$ from EASE Score, a modified Fisher Exact P-Value. **(b)** The down-regulation of selected MSN-specific mRNAs ($n = 4$ control (1 male, 3 females), 6 mutant mice (2 males, 4 females)) in PRC2-deficient neurons is shown. The mRNA expression levels were quantified by qRT-PCR ((*Adora2a*) $P < 0.0001$, t (8) = 14.55; (*Arpp21*) P = 0.0001, t (8)= 6.894; (*Bcl11b*) $P = 0.0004$, t (8) = 5.855; (*Drd1a*) $P < 0.0001$, t (8) = 11.08; (*Drd2*) $P < 0.0001$, t (8) = 11.39; (*Foxp1*) $P = 0.0005$, t (8) = 5.618; (*Gpr6*) $P < 0.0001$, t (8) = 7.507; (*Gpx6*) $P = 0.0008$, t (3) = 14.01; (*Ido1*) $P < 0.0001$, t (8) = 28.94; (*Pde10a*) $P = 0.0125$, t (8) = 3.204; (*Rgs9*) $P < 0.0001$, t (8) = 9.475; (*Rxrg*) $P < 0.0001$, t (8) = 11.02). **(c)** The venn diagram shows a significant enrichment of the previously identified MSN identity genes (Heiman et al., 2008; Lein et al., 2007) among the 119 down-regulated genes in PRC2-deficient MSNs. Significance of the venn diagram was calculated using Chi-square test, $P < 0.0001$. **(d)** The down-regulation of *Drd2* mRNA expression levels within individual PRC2-deficient D2 MSNs was demonstrated by using *in situ* mRNA analysis on brain slices with PRC2-deficient or control MSNs (scale bar 10 μm); the quantification of the total number of *Drd2+* MSNs (left, $P = 0.7882$, t (8) = 0.2844) and the intensity of *Drd2+* mRNA expression per neuron (right, $P = 0.0004$, t (8) = 5.885) are shown ($n = 5$ slides from 2 different animals per genotype, representative image is shown). Data are mean ± SEM. n.s., nonsignificant, $*P \leq 0.05$, $**P \leq 0.01$, $***P \leq 0.001$ from two-tailed unpaired Student *t* test with Welch's correction.

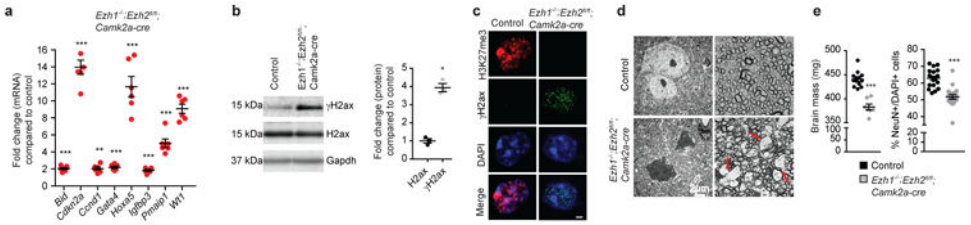

Fig. 5. PRC2 deficiency leads to up-regulation of death-promoting genes and associated neurodegenerative changes in MSNs (a)

Up-regulation of death-promoting genes in PRC2-deficient MSNs (n = 4 control (1 male, 3 females), 6 mutant mice (2 males, 4 females)). The gene expression levels were quantified by qRT-PCR ((*Bid*) P = 0.0003, t (8) = 5.977; (*Cdkn2a*) P < 0.0001, t (5) = 15.64; (*Ccnd1*) P = 0.0027, t (5) = 5.516; (*Gata4*) P = 0.0003, t (8) = 6.018; (*Hoxa5*) P = 0.0003, t (5) = 8.721; (*Igfbp3*) P = 0.0009, t (8) = 5.165; (*Pmaip1*) P = 0.0006, t (5) = 7.617; (*Wt1*) P < 0.0001, t (5) = 14.68). (**b**) PRC2 deficiency leads to increased phosphorylation of γH2Ax in MSNs. The γH2Ax was quantified by Western blot analysis of striatum protein extracts (n = 3 per genotype, experiment has been performed twice, representative image is shown; P = 0.0003, t (4) = 11.34) or **(c)** visualized by immunofluorescence of control or PRC2-deficient MSNs (n = 3 mice per genotype, representative image is shown). One representative MSN nuclei (DAPI, blue; H3K27me3, red; γH2Ax, green) is shown; scale bar 2 μm. **(d)** Electron microscopy images of the striatum of > 6 month-old *Ezh1*$^{-/-}$*; Ezh2*$^{fl/fl}$*; Camk2a-cre* mice show dark cell degeneration and axonal loss (n = 3 animals each (control: 1 male, 2 females; mutant: 3 females), representative images are shown); scale bar 2 μm. **(e)** *Ezh1*$^{-/-}$*; Ezh2*$^{fl/fl}$*; Camk2a-cre* mice show a total brain mass reduction (n = 7 mutant (3 males, 4 females), 13 control mice (7 males, 6 females); P < 0.0001, t (18) = 7.778) and a decrease in total number of NeuN+ neurons over total DAPI+ cells (n = 18 control, 20 mutant slides, 3 mice each (control: 3 males; mutant: 2 males, 1 female); P < 0.0001, t (36) = 5.987) as compared to littermate controls at > 6 months of age. Data are mean ± SEM. *P ≤ 0.05, **P ≤ 0.01, ***P ≤ 0.001 from two-tailed unpaired Student t test with Welch's correction.

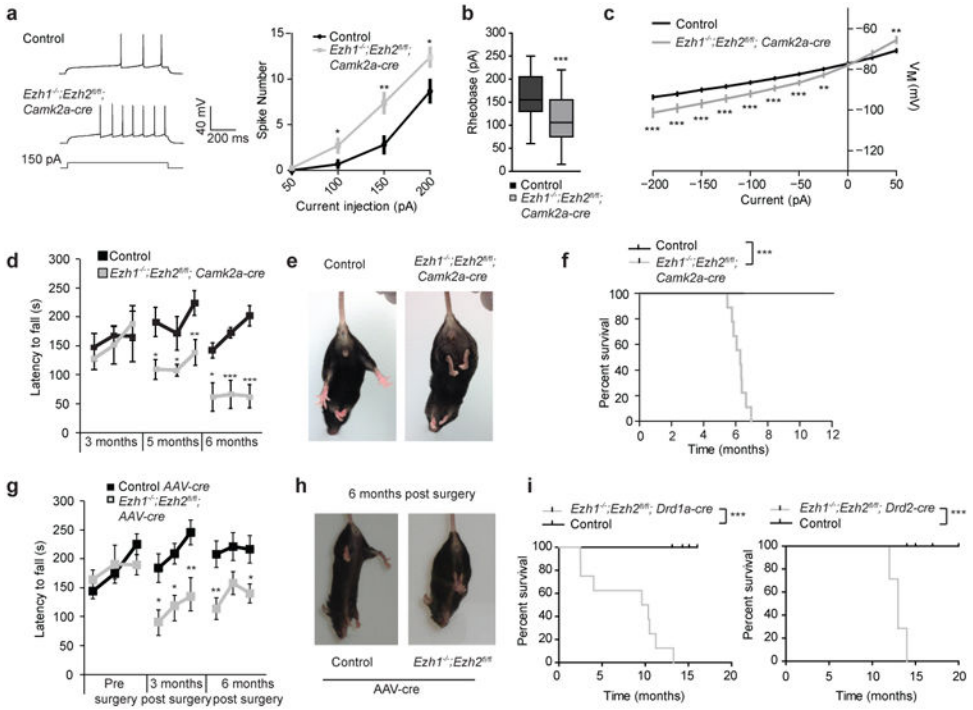

Fig. 6. PRC2 deficiency in adult neurons causes a progressive and fatal neurodegenerative phenotype in mice

(**a**) Representative sample traces of spike numbers obtained by 150 pA current injection in striatal neurons of control and *Ezh1*$^{-/-}$*; Ezh2*$^{fl/fl}$*; Camk2a-cre* mice (left) are shown. Whole-cell quantification of current-induced spike numbers indicate enhanced excitability in Ezh1/Ezh2 deficient MSNs (right, $n = 5$ mice each (2 males, 3 females), 43 cells for control, 40 cells for mutant mice; (100 pA) $P = 0.0148$, t (58) = 2.513; (150 pA) $P = 0.0013$, t (77) = 3.330; (200 pA) $P = 0.0189$, t (81) = 2.396). (**b**) Rheobase of MSNs is shown ($n = 5$ mice each (2 males, 3 females), 43 cells for control, 40 cells for mutant mice; $P < 0.001$, t (80) = 4.272). (**c**) *I-V* relationship of MSNs is shown ($n = 5$ mice each (2 males, 3 females), 43 cells for control, 39 cells for mutant mice; (-200 pA) $P = 0.0012$, t (50) = 3.444; (-175 pA) $P = 0.001$, t (52) = 3.490; (-150 pA) $P = 0.0006$, t (50) = 3.691; (-125 pA) $P = 0.0004$, t (50) = 3.810; (-100 pA) $P = 0.0003$, t (52) = 3.835; (-75 pA) $P = 0.0003$, t (55) = 3.903; (-50 pA) $P = 0.0002$, t (57) = 3.941; (-25 pA) $P = 0.002$, t (67) = 3.212; (0 pA) $P = 0.3635$, t (80) = 0.9139; (25 pA) P = 0.0698, t (59) = 1.847; (50 pA) $P = 0.0026$, t (58) = 3.144). (**d**) Impaired motor balance during the accelerated rotarod test in *Ezh1*$^{-/-}$*; Ezh2*$^{fl/fl}$*; Camk2a-cre* mice at 5 and 6 months of age is shown ($n = 5$ control (2 males, 3 females), 8 mutant mice (2 male, 6 females); interaction $P < 0.0001$, F(1,8) = 4.992; genotype $P = 0.0112$, F(1,8) = 9.25). **(e)** Representative image of hind limb clasping behavior ($n = 5$ control (2 males, 3 females), 8 mutant mice (2 male, 6 females)). (**f**) Kaplan-Meier survival curve is shown ($n =$ 14 mutant (8 males, 6 females), 20 control mice (10 males, 10 females); $P < 0.0001$; χ^2 (1) = 36.28 from Log rank Mantel Cox test). **(g)** Impaired motor balance in *Ezh1*$^{-/-}$*; Ezh2*$^{fl/fl}$*; AAV-cre* mice 3 and 6 months after surgery ($n = 5$ control (3 males, 2 females), 6 mutant mice (4 males, 2 females); $P = 0.0057$, F(1,72) = 12.99). **(g)** Representative image of hind limb clasping behavior ($n = 5$ control (3 males, 2 females), 6 mutant mice (4 males, 2

females)). **(i)** Kaplan-Meier survival curve for *Ezh1*$^{-/-}$*; Ezh2*$^{fl/fl}$*; Drd1a-cre* and *Ezh1*$^{-/-}$*; Ezh2*$^{fl/fl}$*; Drd2-cre* is shown (D1: $n = 8$ mutant (4 males, 4 females), 20 control mice (9 males, 11 females); $P < 0.0001$; χ^2 (1) = 41.01 from Log rank Mantel Cox test; D2: $n = 7$ mutant (3 males, 4 females), 7 control mice (4 males, 3 females); $P = 0.0002$; χ^2 (1) = 13.61 from Log rank Mantel Cox test). Data are mean ± SEM. *$P \leq 0.05$, **$P \leq 0.01$, ***$P \leq 0.001$ from two-tailed Student *t* test or two-way ANOVA with repeated measures.

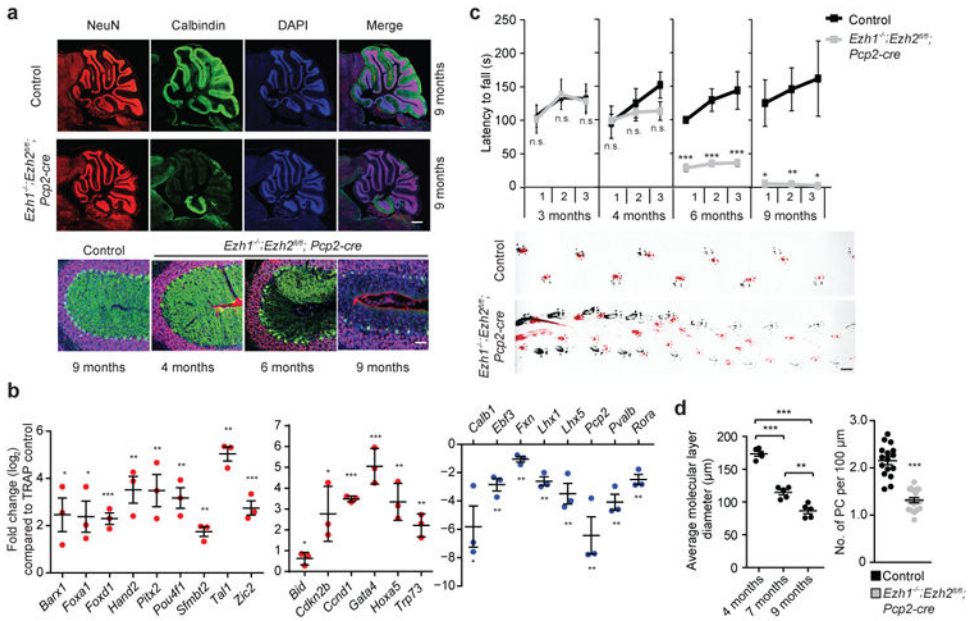

Fig. 7. PRC2 deficiency in Purkinje cells (PC) impairs PC-specific gene expression and function

(**a**) (Top panel) Cerebellar PC were identified using PC-specific calbindin expression (green), NeuN (red), and DAPI (blue), (scale bar, 500 μm). (Bottom panel) Representative images of cerebellar lobule 8 reveal progressive loss of PRC2-deficient PCs (scale bar, 50 μm; $n = 3$ mice per genotype per age). (**b**) PRC2 deficiency in PC is associated with changes in gene expression. The indicated gene expression levels were measured using Translating Ribosome Associated PC-specific mRNA analysis of cerebelli derived from *Ezh1*$^{-/-}$*; Ezh2*$^{fl/fl}$*; Pcp2-cre; Pcp2-TRAP* or control mice ($n = 3$ mice each (2 males, 1 female); (Left) (*Barx1*) $P = 0.026$, t (4) = 3.451; (*Foxa1*) $P = 0.0229$, t (4) = 3.592; (*Foxd1*) $P = 0.0113$, t (2) = 9.336; (*Hand2*) $P = 0.0252$, t (2) = 6.185; (*Pitx2*) $P = 0.0085$, t (4) = 4.818; (*Pou4f1*) $P = 0.0034$, t (4) = 6.205; (*Sfmbt2*) $P = 0.0036$, t (4) = 6.119; (*Tal1*) $P = 0.006$, t (4) = 5.325; (*Zic2*) $P = 0.0009$, t (4) = 8.888; (Center) (*Bid*) $P = 0.0267$, t (4) = 3.425; (*Cdkn2b*) $P = 0.0401$, t (4) = 2.995; (*Ccnd1*) $P < 0.0001$, t (4) = 20.12; (*Gata4*) $P = 0.0096$, t (4) = 10.12; (*Hoxa5*) $P = 0.0054$, t (4) = 5.488; (*Trp73*) $P = 0.0032$, t (4) = 6.342; (Right) (*Calb*) $P = 0.0165$, t (4) = 3.976; (*Ebf3*) $P = 0.0233$, t (2) = 6.438; (*Fxn*) $P = 0.0073$, t (4) = 5.037; (*Lhx1*) $P = 0.0012$, t (4) = 8.273; (*Lhx5*) $P = 0.0409$, t (4) = 4.792; (*Pcp2*) $P = 0.0401$, t (2) = 4.845; (*Pvalb*) $P = 0.0022$, t (4) = 6.954; (*Rora*) $P = 0.0026$, t (4) = 6.696)). (**c**) The progressive loss of motor coordination and balance was determined by the rotarod test ($n = 4$ control (3 males, 1 female), 9 mutant mice (5 males, 4 females); interaction $P = 0.0002$, F(1,11) = 3.626; genotype $P < 0.0001$, F(1.11) = 50.82) (top) and the foot printing assay (bottom) ($n = 6$ mice each (3 males, 3 females), two trials,, representative image is shown; scale bar, 1 cm). (**d**) A decrease in average lobe diameter over time (left, $n = 5$ brain sections; $P < 0.0001$, F(2,12) = 121.2) and the number of Purkinje cells as determined by Nissl staining (right, $n = 3$ mice (16 control, 18 mutant brain slides; $P < 0.0001$, t (32) = 8.541) are shown. Data are mean ± SEM. *$P \leq 0.05$, **$P \leq 0.01$, ***$P \leq 0.001$ from two-tailed Student *t* test with Welch's correction or Two-way ANOVA with repeated measures.